



Norwegian University of  
Science and Technology

# Reliability Evaluation of Energy-Limited Hydro-Electric Generation Systems

**Henrik Jøssund Karlsen**

Master of Energy and Environmental Engineering

Submission date: June 2018

Supervisor: Vijay Vadlamudi, IEL

Norwegian University of Science and Technology  
Department of Electric Power Engineering



# Abstract

Reliability studies are an essential part of power system planning and operation studies. A wide range of reliability indices is used by system planners and operators to ensure successful operation of power systems against random failures both in the planning and operational horizons. In generation system reliability studies, it is usual to consider the energy source for generation as always available. This implies that unavailability of generation is solely on account of a generation unit of the power plant; in the case of hydro generation, if the reservoir is sufficiently large enough to guarantee the availability of energy, through a constant regime of inflows, such modelling is correct. However, stochastic nature of inflows and reservoir limitations make hydro generation energy-limited.

In this thesis, multiple methods for incorporating energy-limited hydro generation units in generation system reliability studies, from the literature, have been examined. Three of the methods have focused on hydro generation units with reservoir limitations, meaning that each hydro unit only has a fixed amount of water available for generation. The *capacity modification method* (CMM) treats the limited hydro units as non-limited, but with a modified capacity depending on the capacity-probability table and the energy distribution of the unit. The same applies to the *forced outage ratio* (FOR) *modification method*, only with a modified probability instead of capacity. The massive benefit of these methods is that they treat the units as non-limited, which means the energy-limited units can easily be implemented in reliability test systems. The *load modification method* (LMM) makes use of the energy-limited units to reduce the load duration curve (LDC), and with the remaining non-limited units calculates the reliability indices. The method produces accurate results, but gets complicated as the number of energy-limited units is increased as this also increases the number of load steps. The methodological approaches are illustrated for simple systems for conceptual clarity.

A model of a run-of-the-river (ROR) power plant for evaluating power system reliability, from the literature, is also examined. The model considers the uncertainties of both river inflows and component failures, where the river inflows and component failures are modeled as a stationary stochastic process by a multiple state Markov model. The stochastic system is solved with linear algebra, and the steady-state probabilities of all capacity states are obtained. The final capacity-probability table represents a ROR power plant well, and can be used in other reliability evaluations. The river inflow values at Solbergfoss in the river Glomma in Norway are used in a case study, and the vast number of river inflow values are reduced by the statistical clustering technique  $k$ -means. The ROR model is then extended, again based on suitable existing literature, to also take into account the modelling of failure rates of all the components of a typical ROR plant.

The CMM and the extended ROR model are utilized on two reliability test systems, the Roy Billinton Test System (RBTS) and IEEE Reliability Test System (IEEE-RTS), to demonstrate the impact on system reliability from energy-limited units. The results show a significant effect from reservoir limited hydro units on the system reliability, and the energy-limited hydro units should thus be included in reliability evaluation. The ROR unit is compared to a conventional unit of the same size. The ROR unit strengthens the reliability, but not as much as the conventional unit; this means if the same reliability output is desired, a larger ROR unit must be used.

# Sammendrag

Pålitelighetsstudier er en betydningsfull del av planleggingen og driften av kraftsystemer. Et bredt spekter av pålitelighetsindekser benyttes av systemplanleggere og operatører for å sikre en vellykket drift av kraftsystemet mot tilfeldige feil både i planleggings- og driftsfasen. I pålitelighetsstudier er det vanlig å anta at energikilden alltid er tilgjengelig. Dette innebærer at utilgjengeligheten av kraftproduksjon skjer utelukkende på grunn av en feil i en produksjonsenhet i kraftverket; ved vannkraftproduksjon, dersom reservoaret er tilstrekkelig stort nok til å garantere tilgjengeligheten av vann, gjennom kontinuerlig innstrømming, er denne antagelsen riktig. Likevel, stokastisk vanninnstrømning og reservoarbegrensninger gjør vannkraftproduksjonen begrenset.

I denne masteroppgaven har flere metoder for å inkludere energibegrensede vannkraftenheter i pålitelighetsstudier, fra litteraturen, blitt undersøkt. Tre av metodene har fokusert på vannkraftenheter med reservoarbegrensninger, noe som betyr at hver enhet kun har en fast mengde vann tilgjengelig for kraftproduksjon. *Kapasitetsmodifikasjonsmetoden* (CMM) behandler de begrensede vannkraftenhetene som ikke-begrensede, men med en modifisert kapasitet, avhengig av kapasitetssannsynlighetstabellen og energidistribusjonen til enheten. Det samme gjelder for *tvungen avbrudd-metoden* (FOR), bare med en modifisert sannsynlighet i stedet for kapasitet. Den massive fordelene med disse metodene er at de behandler enhetene som ikke-begrensede, noe som medfører at de energibegrensede enhetene enkelt kan implementeres i testsystemer knyttet til pålitelighet. *Lastmodifikasjonsmetoden* (LMM) benytter de energibegrensede enhetene til å redusere lastkurven (LDC), mens de resterende, ikke-begrensede enhetene beregner pålitelighetsindeksene. Metoden gir nøyaktige resultater, men blir komplisert ettersom antallet energibegrensede enheter øker, da dette også øker antall trinn i metoden. De tre metodene benyttes i enkle, numeriske eksempler for konseptuell klarhet.

En modell av et elvekraftverk (ROR) for pålitelighetsevaluering undersøkes også. Modellen tar hensyn til usikkerheten knyttet både til elveinstrømning og komponentfeil, der elvinnstrømningen og komponentfeil er modellert som en stasjonær stokastisk prosess med en Markov-modell. Det stokastiske systemet løses med lineær algebra, og de stabile sannsynlighetene for hver kapasitet beregnes. Den endelige kapasitetssannsynlighetstabellen representerer et elvekraftverk godt, og kan brukes i andre pålitelighetsevalueringer. Innløpsverdiene ved Solbergfoss i elven Glomma i Norge blir brukt, og det store antallet innstrømningsverdier er redusert med den statistiske klyngeteknikken  $k$ -means. Videre blir ROR modellen utvidet, igjen basert på passende litteratur, ved å også inkludere strykprosenten til alle komponentene i et typisk elvekraftverk.

CMM og den utvidede ROR-modellen benyttes i to pålitelighetstestsystemer, Roy Billinton Test System (RBTS) og IEEE Reliability Test Test System (IEEE-RTS), for å teste effekten fra energibegrensede enheter på systemets pålitelighet. Resultatene viser en betydelig effekt fra reservoarbegrensede vannkraft-enheter på systemets pålitelighet, og bør derfor inkluderes i pålitelighetsevalueringer. ROR-enheten er sammenlignet med en konvensjonell enhet med samme størrelse. ROR-enheten styrker påliteligheten, men ikke så mye som den konvensjonelle enheten; dette betyr at hvis samme pålitelighetsforbedring er ønsket, må en større ROR-enhet benyttes.

# Preface

This Master's Thesis concludes my Master of Science (MSc) degree in Energy and Environmental Engineering with the Department of Electric Power Engineering at the Norwegian University of Science and Technology (NTNU). The thesis treats concepts related to Power System Reliability (PSR), and is written under the supervision of Associate Professor Vijay Venu Vadlamudi with the Department of Electric Power Engineering at NTNU.

Writing this thesis has given me an excellent introduction to research and academic writing, and I have built a solid foundation for potential future work within the areas of PSR. I would like to thank my supervisor, Associate Professor Vijay Venu Vadlamudi, for his guidance and encouragement. I would also like to express my gratitude to Svein Taksdal at NVE for providing me with historical river inflow data from Solbergfoss.

Trondheim, June 2018

Henrik Jøssund Karlsen



# Contents

Abstract	i
Sammendrag	iii
Preface	v
Table of Contents	vii
Abbreviations	xi
Nomenclature	xiii
List of Tables	xv
List of Figures	xvii
<b>1 Introduction</b>	<b>1</b>
1.1 Background . . . . .	1
1.2 Scope . . . . .	2
1.3 Thesis Structure . . . . .	3
<b>2 Conceptual Background</b>	<b>5</b>
2.1 Generation System Adequacy . . . . .	6
2.2 Loss of Load Indices . . . . .	7
2.2.1 Load Model . . . . .	8
2.2.2 Generation Model . . . . .	8
2.2.3 LOLP . . . . .	10

2.2.4	LOLE . . . . .	11
2.2.5	EENS . . . . .	11
2.3	Literature Review . . . . .	12
2.3.1	Energy Limitation in Analytic Reliability Evaluation . . . . .	12
2.3.2	Markov Models in Reliability Evaluation Considering Energy Limitation . . . . .	14
<b>3</b>	<b>Illustration of Fundamental Methods</b>	<b>15</b>
3.1	Capacity Modification Method . . . . .	15
3.1.1	Numerical Example . . . . .	16
3.2	Load Modification Method . . . . .	20
3.2.1	Numerical Example . . . . .	20
3.3	The Forced Outage Ratio Modification Method . . . . .	27
3.3.1	Numerical Example . . . . .	28
<b>4</b>	<b>Run-of-the-River in Reliability Evaluation</b>	<b>33</b>
4.1	Reliability Evaluation of a Run-of-the-River Power Plant . . . . .	33
4.1.1	River Inflow Model . . . . .	34
4.1.2	Markov Chain Model of the River Inflow . . . . .	39
4.1.3	Small Hydro Plant Generation Model . . . . .	43
4.1.4	Calculation of the Steady State Probabilities . . . . .	45
4.1.5	Calculation of the Reliability Indices . . . . .	48
4.2	Expansion of the ROR Hydro Plant Model . . . . .	48
4.2.1	Structure of a Typical ROR Power Plant . . . . .	49
4.2.2	Two-State Markov Model of the ROR Components . . . . .	50
4.2.3	Markov Model of ROR Power Plant With One Penstock . . . . .	51
4.2.4	Markov model of ROR Power Plant With Several Penstocks . . . . .	52
4.2.5	Final Markov Model of ROR Power Plant . . . . .	54
4.2.6	Combining the ROR Power Plant Model With a River Inflow Model . . . . .	56
4.2.7	Calculation of the Steady State Probabilities . . . . .	56
<b>5</b>	<b>Case Study: Utilizing the Methods in Test Systems</b>	<b>61</b>
5.1	Test Systems . . . . .	61
5.1.1	RBTS . . . . .	61
5.1.2	IEEE-RTS . . . . .	64
5.2	Solbergfoss ROR Power Plant . . . . .	65

<i>CONTENTS</i>	ix
5.3 Adequacy Evaluation . . . . .	66
5.3.1 Reliability Indices for the RBTS . . . . .	66
5.3.2 Reliability Indices for the IEEE-RTS . . . . .	70
<b>6 Conclusions and Future Work</b>	<b>73</b>
6.1 Discussion and Conclusions . . . . .	73
6.2 Improvements and Suggestions for Future Work . . . . .	75
<b>Bibliography</b>	<b>77</b>
<b>A Example of the Recursive COPT Algorithm</b>	<b>81</b>
<b>B Load Data for the Test Systems</b>	<b>85</b>
<b>C Brazilian River Inflow Data</b>	<b>89</b>
<b>D Solbergfoss River Inflow Data</b>	<b>93</b>
<b>E MATLAB Code</b>	<b>99</b>



# Abbreviations

<b>FC</b>	Capacity Factor
<b>CMM</b>	Capacity Modification Method
<b>COPT</b>	Capacity Outage Probability Table
<b>DPL</b>	Daily Peak Load
<b>DPLVC</b>	Daily Peak Load Variation Curve
<b>EAE</b>	Expected Available Energy
<b>EGE</b>	Expected Generated Energy
<b>EU</b>	European Union
<b>EENS</b>	Expected Energy Not Served
<b>FOR</b>	Forced Outage Ratio
<b>F&amp;D</b>	Frequency and Duration
<b>GAF</b>	Generation Availability Factor
<b>HLI</b>	Hierarchical level I
<b>HLII</b>	Hierarchical level II
<b>HLIII</b>	Hierarchical level III
<b>IC</b>	Installed Capacity
<b>IE</b>	Installed Energy

<b>IEEE-RTS</b>	IEEE Reliability Test System
<b>LDC</b>	Load Duration Curve
<b>LOLE</b>	Loss of Load Expectation
<b>LOLP</b>	Loss of Load Probability
<b>LMM</b>	Load Modification Method
<b>OC</b>	Original Case
<b>PV</b>	Photovoltaic
<b>PSR</b>	Power System Reliability
<b>RBTS</b>	Roy Billinton Test System
<b>RES</b>	Renewable Energy Resources
<b>ROR</b>	Run-of-the-River
<b>WPL</b>	Weekly Peak Load
<b>YPL</b>	Yearly Peak Load

# Nomenclature

$x_j$	Capacity on outage in outage state $j$
$P(X \geq x_j)$	Cumulative probability of capacity outage
$p(X)$	Individual probability of event $X$
$IC$	Total installed capacity
$j$	Running index of outage-/assistance states
$p_{up}$	Probability of generating unit being available
$p_{down}$	Probability of generating unit being unavailable
$p_i$	Probability of generating unit being in derated state $i$
$P^{old}(X)$	Cumulative probability of event $X$ before adding a new generating unit to the COPT
$g$	Capacity of generating being added to COPT as a two-state model
$P^{new}(X)$	Updated cumulative probability of event $X$ after adding a new generating to the COPT
$i$	Running index of derated states for a generating unit
$g_i$	Capacity of derated state $i$ for a generating unit being added to COPT as a multi-state unit
$t$	Running index of time increments in a load model
$L_t$	Load level in time increment $t$
$C_i$	Capacity of generating unit un state $i$

$\lambda$	Failure rate
$\mu$	Repair rate
$r$	Repair time
$\lambda_{ij}$	Transition rate between state $i$ and state $j$

# List of Tables

3.1	Capacity probability and energy distribution of Unit#1. . . . .	16
3.2	Capacity probability and energy distribution of Unit#2. . . . .	17
3.3	Load model . . . . .	17
3.4	Modified capacity probability table for Unit#1. . . . .	18
3.5	Modified capacity probability table for Unit#2. . . . .	18
3.6	System COPT after adding Unit#1. . . . .	19
3.7	System COPT after adding Unit#2. . . . .	20
3.8	Load levels and duration for the capacity-modified curve, modified by Unit#1.	21
3.9	Load levels and duration for the capacity-modified curve, modified by Unit#2.	24
3.10	FOR modified capacity-probability table for Unit#1 and Unit#2. . . . .	29
3.11	System COPT after adding FOR modified Unit#1. . . . .	30
3.12	System COPT after adding FOR modified Unit#2. . . . .	31
3.13	Comparison of the EENS from the different modification methods . . . . .	31
4.1	The cluster centroids produced by the k-means technique. . . . .	38
4.2	Number of transitions observed in Figure 4.5. . . . .	40
4.3	Transition rates between the states in Figure 4.5. . . . .	41
4.4	Number of transitions between the clustered inflow states in Figure 4.4. . . .	42
4.5	Transition rates between the clustered inflow states in Figure 4.5. . . . .	42
4.6	The cluster centroids and the generated power for each river inflow cluster. .	44
4.7	Transition intensity matrix of the river inflow in Figure 4.4. . . . .	46
4.8	Probability of generation without considering generator failure. . . . .	47
4.9	Probability of generation considering generator failure. . . . .	47
4.10	Reliability indices of the SHPP generation model. . . . .	48
4.11	Reliability data of the ROR power-plant components . . . . .	58
4.12	Probability of generation from the ROR power plant. . . . .	59

5.1	Generating unit reliability data for RBTS. . . . .	62
5.2	Capacity probability table for the hydro units in RBTS. . . . .	63
5.3	Capacity modified hydro units in RBTS. . . . .	63
5.4	Generating unit reliability data for IEEE-RTS. . . . .	64
5.5	Capacity probability table for the hydro units in IEEE-RTS. . . . .	65
5.6	Capacity modified hydro units in IEEE-RTS. . . . .	65
5.7	The cluster centroids produced by the k-means technique for Solbergfoss. . .	66
5.8	Probability of generation from Solbergfoss power plant. . . . .	66
5.9	LOLE and EENS with energy-limited units for the RBTS. . . . .	67
5.10	LOLE and EENS for different peak loads. . . . .	69
5.11	LOLE and EENS with energy-limited units for the IEEE-RTS. . . . .	71
5.12	Impact on LOLE and EENS in the IEEE-RTS from Solbergfoss ROR. . . . .	71
A.1	Generation system data for recursive COPT procedure. . . . .	81
A.2	COPT after addition of unit 1 . . . . .	82
A.3	COPT after addition of unit 2 . . . . .	82
A.4	COPT after addition of unit 3 . . . . .	83
B.1	Daily load data. . . . .	85
B.2	Weekly load data. . . . .	86
B.3	Hourly load data. . . . .	87
C.1	Monthly mean inflow values of Brazilian river. . . . .	89
C.2	Continued monthly mean inflow values of Brazilian river. . . . .	90
C.3	Continued monthly mean inflow values of Brazilian river. . . . .	91
C.4	Continued monthly mean inflow values of Brazilian river. . . . .	92
D.1	Monthly mean inflow values at Solbergfoss. . . . .	93
D.2	Continued monthly mean inflow values at Solbergfoss. . . . .	94
D.3	Continued monthly mean inflow values at Solbergfoss. . . . .	95
D.4	Continued monthly mean inflow values at Solbergfoss. . . . .	96
D.5	Continued monthly mean inflow values at Solbergfoss. . . . .	97

# List of Figures

2.1	Reliability and its sub-divisions. . . . .	5
2.2	Overview of the basic functional zones and hierarchical levels in a power system. . . . .	6
2.3	Adequacy evaluation at hierarchical level I. . . . .	7
2.4	Basic modelling of HLI adequacy studies. . . . .	8
2.5	Different load models. . . . .	9
3.1	Original, 10MW and 15MW reduction LDC after modification by Unit#1. . . . .	22
3.2	Original, capacity modified and energy modified LDC after modification by Unit#1. . . . .	23
3.3	Original and 10MW reduction LDC after modification by Unit#2. . . . .	25
3.4	Original, capacity modified and energy modified LDC after modification by Unit#2. . . . .	26
4.1	Markov model of river inflow . . . . .	34
4.2	Annual and chronological inflows of a Brazilian river (1931-2004) . . . . .	37
4.3	Difference between the clustered time series and the original one. . . . .	38
4.4	Markov model of the clustered river inflow. . . . .	39
4.5	An example of a chronological inflow order, clustered into three states. . . . .	40
4.6	The first and last three inflow states of the clustered inflow states in Figure 4.2b. . . . .	41
4.7	Generator model . . . . .	43
4.8	ROR generation model with two-state generator model. . . . .	44
4.9	Structure of a typical ROR power plant . . . . .	50
4.10	Two-state Markov model of ROR power plant components . . . . .	51
4.11	Reliability block diagram of a ROR unit with one penstock . . . . .	51
4.12	Reliability block diagram of a ROR power plant with $m$ penstocks . . . . .	53

4.13	Markov model of ROR power plant with $m$ penstocks without considering the failure of the water channel and forebay tank. . . . .	53
4.14	Markov model of ROR power plant with $m$ penstocks considering the failure of the water channel and forebay tank . . . . .	54
4.15	Final reliability block diagram of ROR power plant with $m$ penstocks including shoot and power transformer . . . . .	55
4.16	Final Markov model of the ROR power plant with $m$ penstocks considering the failure of the power transformer . . . . .	55
4.17	Markov model of the combined ROR power plant model and clustered river inflow model. . . . .	57
5.1	The effect limited hydro units have on the reliability indices in the RBTS. . . . .	68
5.2	EENS for three cases of the RBTS. . . . .	70
5.3	The effect limited hydro units have on the reliability indices in the IEEE-RTS. . . . .	72

# Chapter 1

## Introduction

### 1.1 Background

The world's electricity sector is in a state of transition, where decarbonization is a crucial driver in the pursuit of a more sustainable and affordable electricity market. A transition from high-carbon to low-carbon energy resources is necessary to reduce the global CO<sub>2</sub> emissions. To keep the global temperature rise in this century well below 2°C above pre-industrial levels, as was stated in the Paris Agreement [1], a considerable amount of renewable energy resources (RES) must be integrated into the energy mix. This transition is well underway as large wind, solar and hydro projects are put into action around the globe. Especially wind and solar generation has experienced a fantastic growth over the last couple of years. The global installed wind capacity in 2017 was 539 GW, while the global installed solar capacity in 2016 was 306 GW. This was an increase from the previous years of respectively 10% and 32% [2] [3]. The exponential growth of solar energy is expected to last over the next few years, meaning that in the best case scenario almost 1 TW of installed solar power is available in the year 2021 [3]. However, these RES are non-dispatchable, meaning that they can't be turned on or off on demand in order to meet the fluctuating electricity needs. This can make the security of energy supply more difficult, which is why hydro generation will continue to play a significant role in the coming years.

Hydropower has the second lowest greenhouse gas emission per kilowatt hour (behind wind), the highest efficiency and the most extended lifetime of all the techniques for power production [4]. The global installed hydro capacity was 1267 GW in 2017 and provides about

16.6% of the global electricity production [4]. In addition to the benefits already mentioned, hydropower is a low-cost electricity supply and stored hydropower is a valuable system management asset capable of ensuring reliable renewable supply. In fact, hydropower accounts for more than 95% of the worldwide energy storage capacity which means that by absorbing the surplus energy and supplying it when needed, hydropower is vital in balancing the grid and is seen as an enabler of renewables such as wind and solar [4].

As intermittent and variable renewable energy sources such as wind and solar continue to grow in market share, the role of hydropower in the power system is changing. In the 2018 Hydropower Status Survey [4], 91% of the respondents said hydropower would increasingly provide a peaking and support role for power systems over base load services. If hydropower will serve as the balancing load in the future, it is important to consider that hydropower is in fact energy-limited, with the stochastic nature of inflows and reservoir limitations. Obtaining the most correct, easy to implement and efficient methods of incorporating these energy-limited units in reliability assessments is essential as the share of renewables will continue to grow. The focus of this thesis will be to study and investigate different methods of incorporating energy-limited units, from the literature, in the reliability evaluation of electric power systems.

## 1.2 Scope

This thesis will investigate the effect of incorporating energy-limited hydro units in reliability studies. Three of the methods focus on hydro units with reservoir limitations: a capacity modification method, a load modification method, and a probability modification method. These methods can be applied to different types of energy-limited resources, but the focus in this theses is on hydropower for conceptual clarity to understand the potential of these methods. In addition to these methods, a comprehensive Markov model of a run-of-the-river (ROR) power plant is investigated. River inflow values from a Norwegian river are combined with a Markov model of a ROR power plant to gain insight into the effect of ROR units in reliability studies.

The reliability indices applied in this report are based on well-established concepts from the field of power system reliability. These indices include Loss-of-Load Probability (LOLP), Loss-of-Load Expectation (LOLE) and Expected Energy Not Served (EENS). Only HLI-

studies are conducted in this report. The results of the reliability studies are obtained from testing on the Roy Billinton Test System (RBTS) and the IEEE Reliability Test System (IEEE-RTS).

### Contributions

Not much literature is available on reliability evaluation of energy-limited hydro electric generation systems; an important objective of the thesis work is to gather the most important works from the literature in this area in one place for a self-contained overview, and provide a pedagogical clarity to the usage of relevant algorithms, with an aim to replicate the results on standard test systems. Further, river inflow data from a Norwegian river (Glomma) is used to demonstrate the applicability of a ROR-reliability evaluation methodology.

1. The thesis presents a conceptual clarity of the different methods of incorporating energy-limited units in reliability studies. Through a detailed explanation of the methods available in the literature, the strengths and weaknesses of the methods are understood, along with the ease of implementing the methods for large generation systems.
2. A comprehensive model of a ROR power plant, based on a suitable integration of contents from two different papers from the literature is investigated, and the effect of ROR units on power system reliability is evaluated.
3. The impact of appropriate modelling of energy-limited units for power system reliability evaluation, in terms of different reliability indices - LOLE and EENS, is demonstrated through case studies on RBTS and IEEE-RTS.
4. Scripts have been developed in MATLAB to implement the studied algorithms in the case studies. These scripts are released for further internal use and research at the Department of Electric Power Engineering, NTNU.

## 1.3 Thesis Structure

Chapter 1 - *Introduction*, provides the background for the thesis and introduces the reader to the scope and the contributions of the thesis.

Chapter 2 - *Conceptual Background*, presents the fundamental concepts of power system reliability and an overview of the previous work from literature on integrating energy-limited

units in reliability evaluation.

Chapter 3 - *Illustration of Fundamental Methods*, presents three methods for incorporating energy-limited units in reliability evaluation studies, including detailed numerical examples.

Chapter 4 - *Run-of-the-River in Reliability Evaluation*, presents a comprehensive Markov model of a ROR power plant and explains how the reliability evaluation of energy-limited ROR hydro-electric generation systems is conducted. The large amount of river inflow values are reduced by applying the  $k$ -means clustering technique.

Chapter 5 - *Case Study: Utilizing the Methods in Test Systems*, applies the studied methods to the test systems RBTS and IEEE-RTS.

Chapter 6 - *Conclusions and Future Work*, discusses and draws conclusions from Chapter 5, including suggestions for future work.

The thesis builds on a specialization project undertaken during Autumn 2017. In order to make the thesis self-contained, for narrative clarity, portions of the specialization project report have been extensively made use of in the presentation of Chapters 2 and 3.

# Chapter 2

## Conceptual Background

The function of the power system is to supply its customers with electrical energy as economically as possible with continuity and quality. That the electrical energy delivered in the power system is enough to supply demand at all times and delivered with acceptable standards is known as power system reliability (PSR). PSR is a comprehensive term but is usually divided into two sub-divisions as shown in Figure 2.1: Adequacy and Security [5]. In the following chapter, an explanation of fundamentals of generation system adequacy is given. The chapter is concluded with a literature review of the important topics in the thesis.

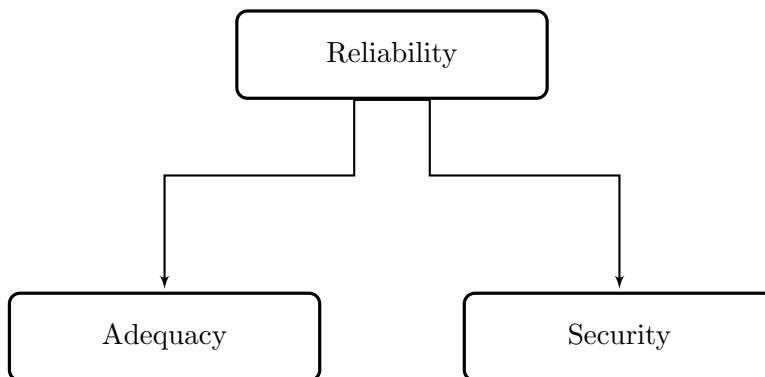


Figure 2.1: Reliability is usually divided into two sub-divisions: Adequacy and Security, adapted from [5].

## 2.1 Generation System Adequacy

System adequacy is defined in [5] as *"...the existence of sufficient facilities within the system to satisfy the consumer load demand"*. Examples of these facilities are the transmission and distribution networks, which makes sure the energy is delivered to the consumer load points, and generation facilities, which make sure there is sufficient generated energy. Adequacy is associated with static conditions and does not include system disturbances. How the system can respond to disturbances arising in the system is known as system security, and is not covered in this thesis. Since the power system is such a large and complex system it is usually divided into three segments defined as functional zones: Generation facilities, Transmission facilities, and Distribution facilities. These zones can be combined to give hierarchical levels as shown in Figure 2.2.

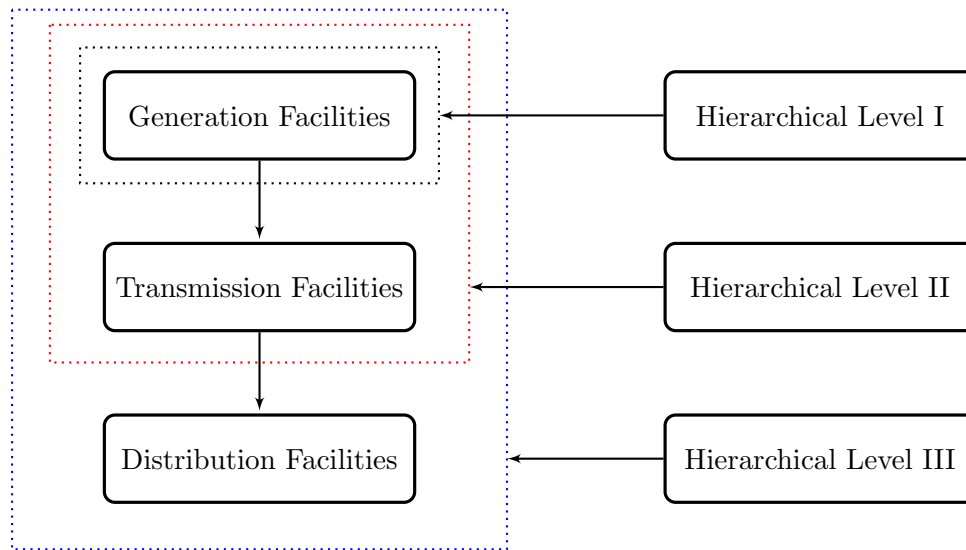


Figure 2.2: Overview of the basic functional zones and hierarchical levels in a power system, adapted from [6].

All the different hierarchical levels can be used for adequacy evaluation. Hierarchical level I (HLI) considers only the generation facilities in the system. At this level, the total system generation is studied to check its adequacy to meet the total system load as seen in Figure 2.3. Hierarchical level II (HLII) considers both generation and transmission facilities, while Hierarchical level III (HLIII) considers all three functional zones. In this thesis, only adequacy evaluation at HLI is treated, also known as generation system adequacy or simply generation adequacy.

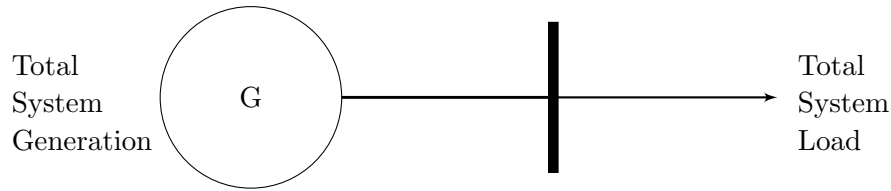


Figure 2.3: Adequacy evaluation at hierarchical level I, adapted from [6].

## 2.2 Loss of Load Indices

When performing a generation adequacy evaluation, one wants to obtain an indication of the performance of the system. A systems performance is evaluated by calculating a given reliability index and comparing it to a criterion. The basic approach to calculating reliability indices for a power system is shown in Figure 2.4. It consists of three parts: a load model, a generation model, and a risk model. A risk model is obtained by convolving a load model with a generation model. The load model is usually either the daily peak load variation curve (DPLVC) or the load duration curve (LDC) to show the variations of the load. The most basic generation model is the capacity outage probability table (COPT), which presents the capacity outage states with their corresponding probabilities. The risk model is evaluated by adequacy indices. There are two types of adequacy indices for HLI studies: the basic indices and the severity-based indices. The basic indices reflect the probability, frequency or duration of losing the load, but not the amount of load lost, e.g., LOLP. The severity-based indices include also the amount of load lost, e.g., EENS. For the calculation of indices, probabilistic methodologies are preferred over deterministic ones [6].

There are two methods of obtaining adequacy indices. The analytical method involves applying direct analytical calculations for obtaining indices such as LOLE, LOLP, EENS and frequency and duration (F&D) indices. The other possibility is a simulation method using Monte Carlo simulation.

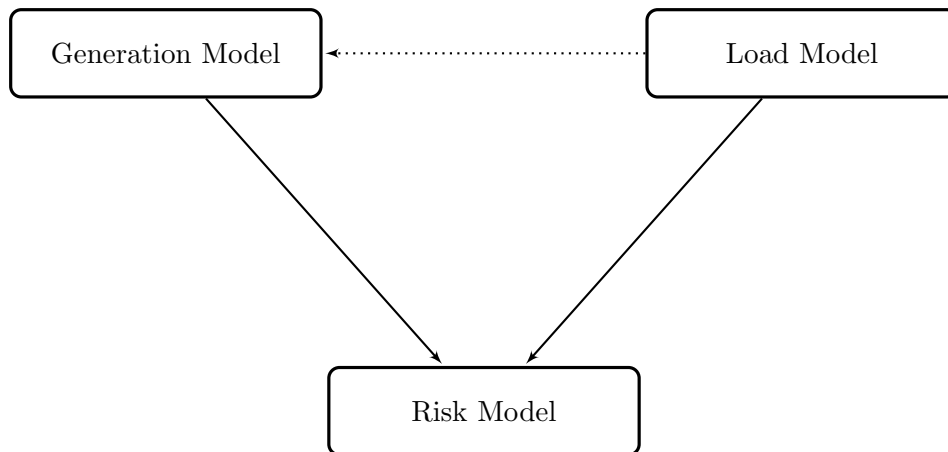


Figure 2.4: Basic modelling of HLI adequacy studies, adapted from [6].

### 2.2.1 Load Model

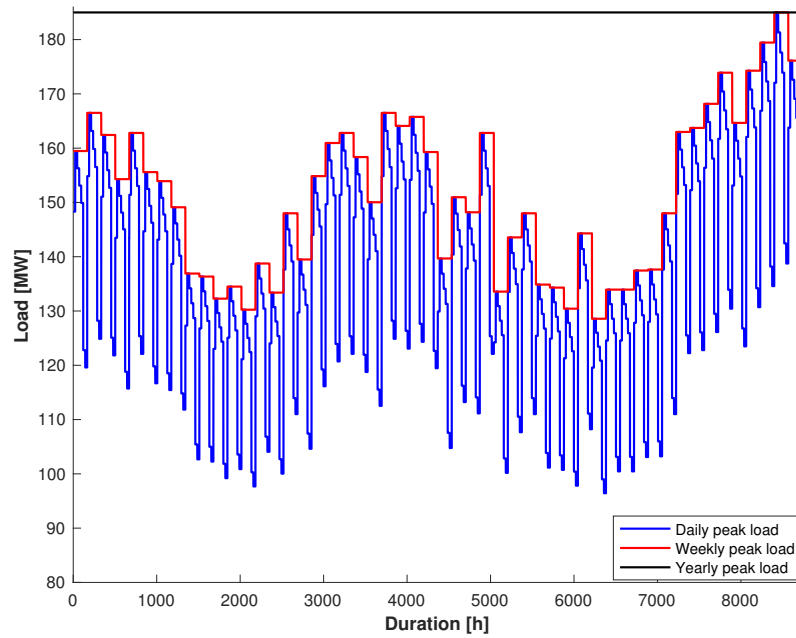
The application of the system load model is to represent the system load for a period, e.g., a week or a year. The simplest load model is where its daily peak load represents each day. If the individual peak loads are arranged in descending order, the DPLVC is obtained. Since only one value represents each day, the amount of data is relatively small. This can improve the computation time but may produce inaccurate results due to the pessimistic models. A more realistic model can be obtained by using individual hourly load values. This results in more data but improves the results as the daily load variations are included. By arranging the individual hourly load data in a descending order, the LDC is obtained. Two different load models are found in Figure 2.5.

### 2.2.2 Generation Model

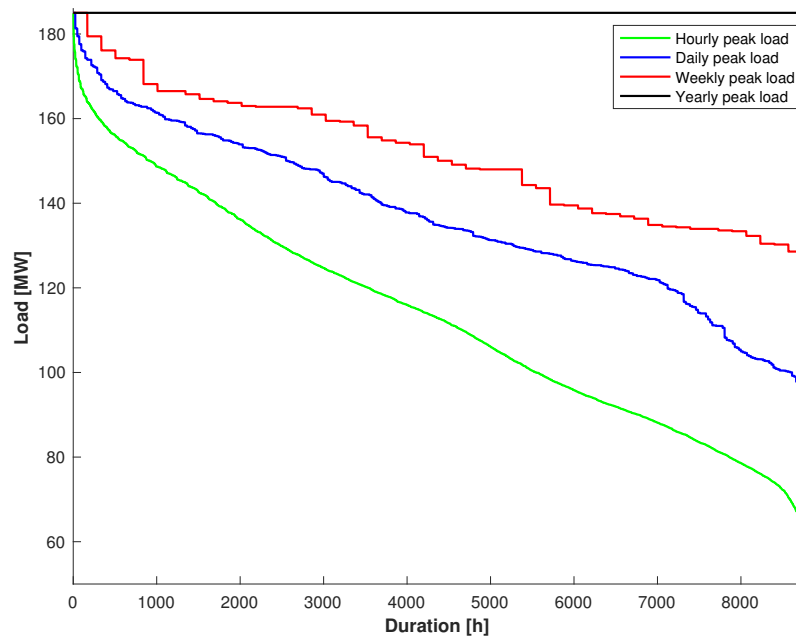
The generation model used in the loss of load approach is the COPT. The COPT is a table made up of all the states of the system, where each state is represented by an amount of generation outage,  $x_j$ . The table also includes the cumulative probability of having an outage greater than or equal to  $x_j$ . The cumulative probability is calculated from:

$$P(X \geq x_j) = \sum_{X=x_j}^{IC} p(X) \quad (2.1)$$

where  $P(X \geq x_j)$  is the cumulative probability,  $p(X)$  is the individual probability of each generator state,  $x_j$  is the generation outage, and  $IC$  is the installed capacity of the system.



(a) Chronological load levels for daily, weekly and yearly peak loads. The load data are from the RBTS with a peak load of 185 MW.



(b) Load duration curves for hourly, daily, weekly and yearly peak loads. The load data are from the RBTS with a peak load of 185 MW.

Figure 2.5: Different load models.

The generation system is made up of generators with two or more states. If the unit has more than two states the unit is said to be a multi-state unit, where the states are called derated states. A unit with two states is the simplest, where the unit is either up or down. When the unit is down, the generator is not working and the individual probability is denoted  $p_{down}$ . This probability is usually called the forced outage ratio (FOR) of the generator. When the unit is up, the generator is working and the individual probability is denoted  $p_{up}$ . The COPT is created by adding each generator one at a time, convolving the capacity states of each unit with the states already added to the COPT.

A recursive algorithm [6] can be used to build the COPT. The cumulative probability after a two-state unit is added given by:

$$P^{new}(X \geq x_j) = (1 - p_{down}) \cdot P^{old}(X \geq x_j) + p_{down} \cdot P^{old}(X \geq x_j - g) \quad (2.2)$$

where  $P^{new}(X \geq x_j)$  is the cumulative probability after the unit is added,  $P^{old}(X \geq x_j)$  is the cumulative probability before the unit is added,  $g$  is the capacity of the unit and  $x_j$  is the generation outage. The above expression is initialized by:

$$P^{old}(X \geq x_j) = \begin{cases} 1 & \text{for } x_j \leq 0 \\ 1 & \text{for } x_j - g \leq 0 \end{cases} \quad (2.3)$$

Modification of Equation (2.2) to include multi-state units can be accomplished as follows:

$$P^{new}(X \geq x_j) = \sum_{i=1}^n p_i \cdot P^{old}(X \geq x_j - g) \quad (2.4)$$

where  $n$  is the number of states,  $p_i$  is the individual probability of state  $i$ . A small example is provided in Appendix A to demonstrate how to obtain a system COPT from the recursive COPT algorithm.

### 2.2.3 LOLP

The loss-of-load probability is the probability of the system load exceeding the available generating capacity at a specified time increment. The LOLP is obtained by combining the load model with the COPT and can be calculated by:

$$\text{LOLP} = P(X > IC - L_t) \quad (2.5)$$

where  $L_t$  is the load for a specified time increment.

### 2.2.4 LOLE

The loss-of-load expectation is the most widely used criterion in generation-planning studies [5]. The LOLE value indicates the expected number of hours or days where load demand is not met. In literature, the terms LOLP and LOLE are often used interchangeably [7], as LOLP is a part of the LOLE-calculation procedure. The LOLE can be calculated as:

$$\text{LOLE} = \sum_{t=1}^{365} P(X > IC - L_t) \cdot \Delta T \quad (2.6)$$

where  $\Delta T$  is the time increment and  $t$  is the load point. In Equation (2.6) the unit is days/year, but there is also possible to use other units if desired.

### 2.2.5 EENS

The problem with LOLE is that it treats every amount of generation deficiency the same. There is no difference if the generation deficiency is 10 MW or a 100 MW, the calculation results in the same LOLE value. The EENS measures the amount of energy expected not to be served and thus evaluates the severity of the deficiency better than LOLE.

The EENS of a system can be calculated by combining the system COPT with the system load. Imagine that the black line in Figure 2.5b is the installed capacity of the system, and the blue LDC is the load. For every outage of generation, the IC-line drops down equal to the amount of generation lost. Let's say 25 MW of generation is lost. The IC-line moves down to 160 MW, but the load stays the same. The area below the LDC and above the IC-line is the amount of energy curtailed by the capacity outage. The EENS can be calculated by Equation (2.7):

$$\text{EENS} = \sum_{j=1}^n E_j \cdot P(X = x_j) \quad (2.7)$$

where  $E_j$  is the energy curtailed by a capacity outage,  $x_j$ ,  $P(X = x_j)$  is the probability of capacity outage  $x_j$  and  $n$  is the number of possible outage states.

## 2.3 Literature Review

The application of probability methods in power system reliability evaluation can be traced back as far as to the 1930s. According to [8], a few of the basic concepts in generation system adequacy were first proposed in 1947, including the "Loss of Load Approach" and the "Frequency and Duration of Outage Approach". These methods have been extended and modified since then, for instance in 1958 [8], but the groundwork was from 1947. As the bibliographies in [8], [9], [10], [11], [12], [13] and [14] show, there is an enormous amount of published material in this field. The focus of this literature review is only on the inclusion of energy limited units, Markov models and clustering approaches in generation system adequacy studies.

### 2.3.1 Energy Limitation in Analytic Reliability Evaluation

Even though there was a lot of published material on the subject of generation system adequacy before the 1980s, most of the papers did not include energy limitation in the evaluation. The focus of the papers was instead on unit forced outages and uncertain load requirements. But as the authors of [15] noted in 1978: "*the era of abundant energy is disappearing and that limitations must be included in conventional studies.*". In the paper [15], three different types of energy limitation were considered: units with large amount of storage, medium amount of storage and no storage at all. The large storage is able to rely on the stored energy for a few days, while the medium storage is able to store enough to use for daily peak demand. The different energy limitations considered in the paper were formulated with hydraulic facilities in mind, but the authors stress that these situations may also arise with gas and oil-fired units.

The adequacy indices used are EENS and Energy Index of Reliability (EIR), and are obtained by convolving a COPT with a load model, as was explained in Section 2.2. For the case with an energy limited unit with no reservoir, in this case a ROR unit, the unit is treated like a conventional unit, only with a few extra derated states. Since the rate of water flow determines the capacity of the unit, the capacity distribution of the unit must be correlated with the river flow rate probability distribution. The ROR unit in [15] has only four capacity states and thus only four river flow rates, which is a bit low for a river, see Figure 4.2b. For the cases with medium and large amounts of storage a "peak-shaving" technique is applied,

termed the Load Modification Method, which is thoroughly explained in Section 3.2. The advantage of this method is that it makes it possible to incorporate energy limitation in adequacy evaluation in a pretty straightforward way, but when the number of limited units is increased the number of load steps can be cumbersome.

Following the years after the Harrington and Billinton paper from 1978 [15] not many papers were published focusing on energy limited hydro units in generation system adequacy studies. In 1987 Chanan Singh and Quan Chen [16] published a paper on reliability modeling of generation systems including energy limited units. The authors extend a previous paper [17] on F&D indices in generation capacity reliability evaluation to also include energy limited units. They look at three different cases of limited energy: uncontrolled hydro, partially base loaded and partially peak-shaving hydro, and controlled hydro. The method used is the 'Equivalent Load Method' [18], where each unit model is viewed as a load model with state capacities represented by negative load values and combined with the load model. This method is an alternative to the 'Conventional Method' [17] and a more efficient one, as it is not necessary to set up a system capacity model.

A paper on load modification was published in 1987 by Billinton and Cheung [19]. The method presented in the paper extends the basic ideas from [15] to create a distinctive procedure to determine the generation adequacy and production cost of a single system and of an interconnected system.

In 1991, Quan Chen [20] published a paper that compared two analytical methods for evaluating generation system adequacy including energy limited units. The two methods were the F&D method and the FOR modification method [21]. In the FOR modification method, the effect of the unit's energy limitation is reflected by modifying the unit forced outage rate and treating the energy limitation as an equivalent failure. The details of the method are carefully explained in Section 3.3.

In 2016, a new analytical technique for incorporating base loaded energy limited hydro units was proposed by Bagen *et al.* [22]. This technique is quite similar to the FOR modification method [21], but instead of modifying the capacity state probabilities the capacities itself were modified. The method is compared to the load modification method and the indices compared are the EENS and LOLE. The two methods produce the same results, however, as the number of energy-limited units increases the capacity modification method is less cumber-

some than the load modification method. A detailed description of the capacity modification method is found in Section 3.1.

### 2.3.2 Markov Models in Reliability Evaluation Considering Energy Limitation

The analytical methods mentioned above are quite simple to use and helpful since the energy limitation of a unit can easily be incorporated. However, as the amount of RES in power systems are increasing, reliability indices should be calculated in a more accurate way than the conventional approaches. The inherent uncertainty associated with RES calls for new stochastic modelling approaches to measure the impacts of these RES in power systems. This is often made possible by Markov modelling of both the energy source and the power plant.

Not many papers address the energy source reliability problem considering hydro generation. A few papers [23, 24, 25, 26] focusing on wind generation was helpful in the modelling of the water flow. In [23], a Markov model for the probabilistic representation of wind farms generation for reliability studies was presented. The model combines the stochastic characteristic of wind speed with failure and repair rates of wind turbines. A Markovian approach to model the energy production and power availability of a wind turbine was proposed in [24]; the paper is especially helpful in obtaining a clear understanding of how transition rates between clustered states are obtained. In [25] and [26] a frequency and duration concept has been used in the analysis of wind farms, similar to the method described in Chapter 4. A Markov model of hydro plants combining the uncertainties of river inflows and generating units are proposed in [27] and [28]. How to obtain these models are thoroughly investigated in Chapter 4.

# Chapter 3

## Illustration of Fundamental Methods

Not much literature is available on reliability evaluation of energy-limited hydro-electric generation systems; an important objective of the thesis work is to gather the most important works from the literature in this area in one place for a self-contained overview, and to provide a pedagogical clarity to the usage of relevant algorithms, with an aim to replicate the results on standard test systems. Accordingly, three prominent methods that deal with reliability evaluation of systems containing hydro units with reservoir limitations have been identified: the capacity modification method (CMM), the load modification method (LMM), and the forced outage ratio (FOR) modification method. The details of these methodological approaches are illustrated for simple systems in this chapter to provide conceptual clarity on fundamental aspects of reliability evaluation of energy-limited hydro-electric generation systems.

### 3.1 Capacity Modification Method

The CMM was first proposed in [22], and the Equations (3.1)-(3.4) are from the mentioned paper. In this method, the energy-limited units can be treated as both base loading units and peak-shaving units. The approach for using the limited units as base loading units are described in the following. The expected energy output from this unit is:

$$\text{Expected Energy} = \sum_{i=1}^N C_i p_i T \quad (3.1)$$

where  $C_i$  is the capacity of the unit in state  $i$ ,  $p_i$  is the corresponding probability, and  $T$  is the duration time for the unit. Since the units are serving as base load, they are needed all

the time, and thus  $T$  is equal to the length of the period under study. The modified capacity due to the energy-limitation for each state of the unit is calculated as follows:

$$C'_i = \frac{C_i \cdot \text{Available Energy}}{\text{Expected Energy}} \quad (3.2)$$

where  $C'_i$  is the modified capacity at state  $i$ . The available energy is calculated from:

$$\text{Available Energy} = \sum_{j=1}^M E_j P_{E_j} \quad (3.3)$$

where  $E_j$  is the energy level of the limited unit,  $P_{E_j}$  is the corresponding probability and  $M$  is the number of levels in the energy distribution. By inserting Equation (3.2) into Equation (3.1) the expected energy after the capacity modification is obtained:

$$\begin{aligned} \text{Expected Energy}' &= \sum_{i=1}^N C'_i p_i T = \sum_{i=1}^N \left( \frac{C_i \cdot \text{Available Energy}}{\text{Expected Energy}} p_i \right) T \\ &= \frac{\text{Available Energy}}{\text{Expected Energy}} \cdot \sum_{i=1}^N (C_i p_i) T = \text{Available Energy} \end{aligned} \quad (3.4)$$

As seen from Equation (3.4) the expected energy from the energy-limited unit after modifying the capacity is equal to the available energy.

### 3.1.1 Numerical Example

The procedure of the CMM is illustrated with a simple numerical example. There are two energy-limited units in this system and a simple two-step load. The data for the energy-limited units are shown in Tables 3.1-3.2 and are taken from [15]. The data for the simple load model is shown in Table 3.3.

Table 3.1: Capacity probability and energy distribution of Unit#1.

<u>Capacity probability</u>		<u>Energy distribution</u>	
Capacity [MW]	Probability	Energy [MWh]	Probability
0.0	0.03	200.0	0.3
10.0	0.25	350.0	0.5
15.0	0.72	500.0	0.2

Table 3.2: Capacity probability and energy distribution of Unit#2.

<u>Capacity probability</u>		<u>Energy distribution</u>	
Capacity [MW]	Probability	Energy [MWh]	Probability
0.0	0.04	70.0	0.4
10.0	0.96	150.0	0.6

Table 3.3: Load model

Load [MW]	Duration [h]
60.0	20
40.0	80

### Capacity-modification of Unit#1

Since the units are base loaded, the duration for which the units are on is equal to the duration of the load model, which is 100 h. Using the data from Table 3.1, the expected and available energy of Unit#1 are calculated from Equations (3.1) and (3.3):

$$\text{Expected Energy}_1 = (0.0 \cdot 0.03 + 10.0 \cdot 0.25 + 15.0 \cdot 0.72) \cdot 100 = 1330 \text{ MWh}$$

$$\text{Available Energy}_1 = (200.0 \cdot 0.3 + 350.0 \cdot 0.5 + 500.0 \cdot 0.2) = 335 \text{ MWh}$$

As both the expected and available energy are obtained for Unit#1, the process of modifying the units' generation capacity can start. The modified capacity due to the energy-limitation is calculated by applying Equation (3.2). For the 15 MW, 10 MW and 0 MW capacity states, the modified capacities are:

$$C'_{15\text{MW}} = \frac{C_{15\text{MW}} \cdot \text{Available Energy}_1}{\text{Expected Energy}_1} = \frac{15 \cdot 335}{1330} = 3.778195489 \text{ MW}$$

$$C'_{10\text{MW}} = \frac{C_{10\text{MW}} \cdot \text{Available Energy}_1}{\text{Expected Energy}_1} = \frac{10 \cdot 335}{1330} = 2.518796992 \text{ MW}$$

$$C'_{0.0\text{MW}} = \frac{C_{0.0\text{MW}} \cdot \text{Available Energy}_1}{\text{Expected Energy}_1} = \frac{0.0 \cdot 335}{1330} = 0.00000000 \text{ MW}$$

The final modified capacity probability table for Unit#1 is shown in Table 3.4. As seen from the table, the probabilities for each capacity state are the same as before the modification.

Table 3.4: Modified capacity probability table for Unit#1.

Capacity [MW]	Probability
0	0.03
2.518796992	0.25
3.778195489	0.72

### Capacity-modification of Unit#2

The same approach can be used to capacity-modify Unit#2. Using the data from Table 3.2, the expected and available energy of this unit are calculated as:

$$\text{Expected Energy}_2 = (0.0 \cdot 0.04 + 10.0 \cdot 0.96) \cdot 100 = 960 \text{ MWh}$$

$$\text{Available Energy}_2 = (70.0 \cdot 0.4 + 150.0 \cdot 0.6) \cdot 100 = 118 \text{ MWh}$$

The modified capacities for the 10 MW and 0 MW states of Unit#2 are:

$$C'_{10\text{MW}} = \frac{C_{10\text{MW}} \cdot \text{Available Energy}_2}{\text{Expected Energy}_2} = \frac{10 \cdot 118}{960} = 1.229166667 \text{ MW}$$

$$C'_{0.0\text{MW}} = \frac{C_{0.0\text{MW}} \cdot \text{Available Energy}_2}{\text{Expected Energy}_2} = \frac{0.0 \cdot 118}{960} = 0.0000000 \text{ MW}$$

The final modified capacity probability table for Unit#2 is shown in Table 3.5.

Table 3.5: Modified capacity probability table for Unit#2.

Capacity [MW]	Probability
0	0.04
1.229166667	0.96

### Calculation of EENS

After the modified capacities have been obtained, the EENS from this two-unit system can

be calculated. Before any of the units are added to the system, there is no generation to serve the load demand. Thus there is a probability of 1.0 of a capacity of 0 MW, and the EENS is equal to the area below the load curve of Table 3.3, shown as the original load duration curve in Figure 3.1.

$$\text{EENS}_0 = 4400 \text{ MWh} \cdot 1.0 = 4400 \text{ MWh}$$

Unit#1 is added first. The COPT after the addition of Unit#1 is given in Table 3.6. By convolving the COPT and the load model (blue curve in Figure 3.1), the EENS for the system at this level is calculated from Equation(2.7):

$$\text{EENS}_1 = 4022.180451 \cdot 0.72 + 4148.120301 \cdot 0.25 + 4400 \cdot 0.03 = 4065 \text{ MWh}$$

where 4022.180451, 4148.129391 and 4400 MWh are values of energy curtailed due to generation outage of 0 MW, 2.518796992 MW and 3.778195489 MW, respectively.

Table 3.6: System COPT after adding Unit#1.

State 'j'	Capacity outage $x_j$ [MW]	Individual probability $p(X = x_j)$	Cumulative probability $P(X \geq x_j)$
1	0	0.72	1.0
2	2.518796992	0.25	0.28
3	3.778195489	0.03	0.03

Next, Unit#2 is added to the system. The updated COPT is given in Table 3.7. Convolving the updated COPT with the load model results in the following EENS:

$$\begin{aligned} \text{EENS}_2 = & 4400 \cdot 0.0012 + 4277.083333 \cdot 0.0288 + 4148.120301 \cdot 0.01 + 4025.203634 \cdot 0.24 \\ & + 4022.180451 \cdot 0.0288 + 3899.263784 \cdot 0.6912 = 3947 \text{ MWh} \end{aligned}$$

Table 3.7: System COPT after adding Unit#2.

State 'j'	Capacity outage $x_j$ [MW]	Individual probability $p(X = x_j)$	Cumulative probability $P(X \geq x_j)$
1	0	0.6912	1.0
2	1.229166667	0.0288	0.3088
3	2.518796992	0.2400	0.2800
4	3.747963659	0.0100	0.0400
5	3.778195489	0.0288	0.0300
6	5.007362156	0.0012	0.0012

## 3.2 Load Modification Method

The LMM is another method to incorporate energy-limited units in a system and is used in several papers including [15], [19], and [22]. As the name suggests, in this method it is the load that is modified. The modification consists of two steps:

1. The first step is to capacity-modify the LDC. The units are first treated as energy-unlimited. For each capacity state of the added unit, an additional LDC is obtained, where the LDC is reduced by an amount equal to the capacity of this state, see Figure 3.1.
2. The second step is to energy-modify the LDC. Once the capacity-modified LDC is obtained, the energy-limitations of the unit are considered. Each load level in the capacity-modified LDC is adjusted to the available and expected energy, see Figure 3.2.

### 3.2.1 Numerical Example

The first step is to capacity-modify the load by Unit#1. The data for the load and for the units are the same as before. Unit#1 has 3 states, 0 MW, 10 MW and 15 MW, the original and additional LDCs are shown in Figure 3.1. The possible load levels can be read in column number 1 in Table 3.8. The duration of the different load levels for the capacity modified curve is calculated from Equation (3.5), given in [15]:

$$D(L) = \sum_{i=1}^N d_i(L) \cdot P_i \quad (3.5)$$

where  $D(L)$  is the duration of load  $L$  on the capacity modified curve,  $N$  is the number of capacity states of the unit,  $P_i$  is the probability of capacity state  $i$  and  $d_i(L)$  is the duration of load  $L$  on the original LDC when reduced by  $C_i$  MW. The duration of each load level for the capacity modified curve can be read from column 5 in Table 3.8.

Table 3.8: Load levels and duration for the capacity-modified curve, modified by Unit#1.

Load	Duration on original LDC	Duration on original LDC reduced by 10MW	Duration on original LDC reduced by 15MW	Duration on capacity modified curve
60	20	0	0	0.6
50	20	20	0	5.6
45	20	20	20	20
40	100	20	20	22.4
30	100	100	20	42.4
25	100	100	100	100

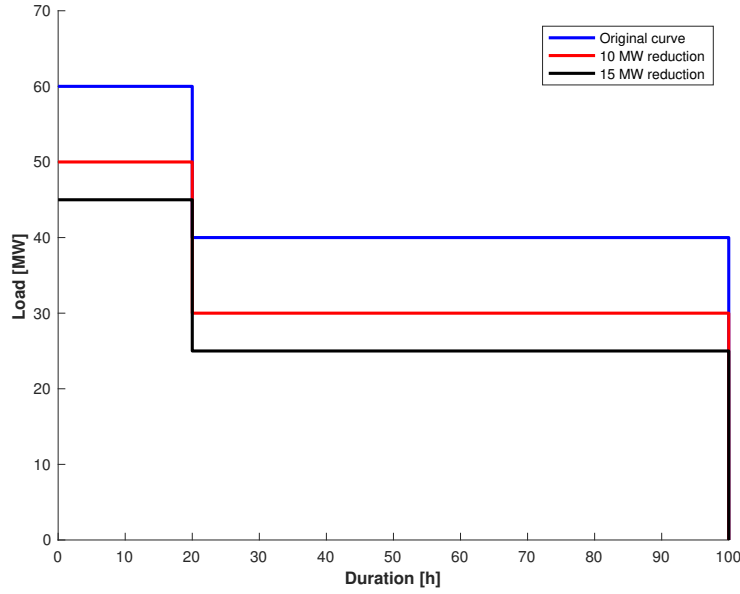


Figure 3.1: Original, 10MW and 15MW reduction LDC after modification by Unit#1.

The final capacity modified curve can be seen in Figure 3.2. After the capacity modified curve has been obtained, the second stage of the LMM can begin. There are normally two approaches regarding the energy modification. One is to use the limited unit to peak shave the LDC, that is to reduce the largest load in the system. The other approach is to use the limited unit for base load, thus reducing the load for the entire period. In this example, the limited units are used for base load.

To obtain the load levels in the final energy-modified curve, Equation (3.6) is used, given in [22]:

$$L_e(i) = L_o(i) - [L_o(i) - L_c(i)] \cdot \frac{\text{Available Energy}}{\text{Expected Energy}} \quad (3.6)$$

where  $i$  is the time interval,  $L_e(i)$  is the load level at time interval  $i$  for the energy-modified curve,  $L_o(i)$  is the load level for the original curve and  $L_c$  is the load level at the capacity modified curve. The available and expected energy are calculated as in Equations (3.3)-(3.1). By applying Equation (3.6), the load levels for the energy-modified curve are:

$$L_e(1) = 60 - [60 - 60] \cdot \frac{335}{1330} = 60.00$$

$$L_e(2) = 60 - [60 - 50] \cdot \frac{335}{1330} = 57.48$$

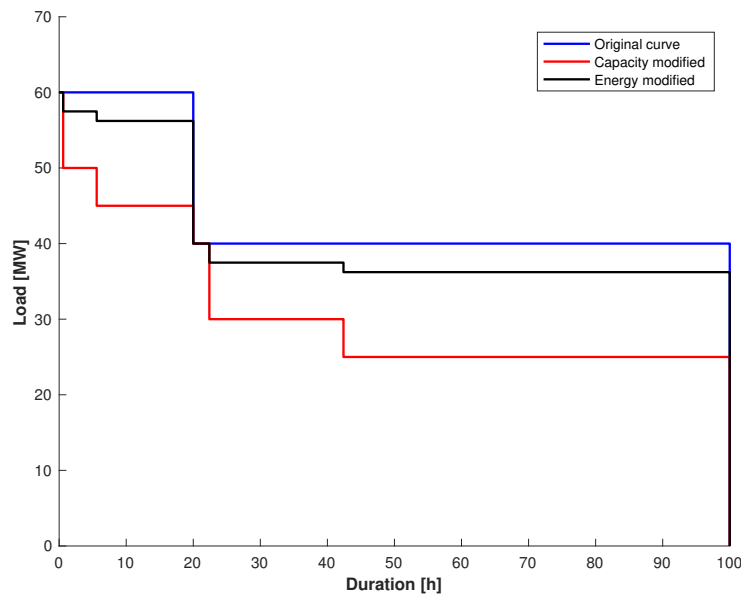


Figure 3.2: Original, capacity modified and energy modified LDC after modification by Unit#1.

$$L_e(3) = 60 - [60 - 45] \cdot \frac{335}{1330} = 56.22$$

$$L_e(4) = 40 - [40 - 40] \cdot \frac{335}{1330} = 40.00$$

$$L_e(5) = 40 - [40 - 30] \cdot \frac{335}{1330} = 37.48$$

$$L_e(6) = 40 - [40 - 25] \cdot \frac{335}{1330} = 36.22$$

The duration of the energy-modified curve is the same as for the capacity-modified curve. Plotting every energy-modified load level with the duration of the capacity-modified LDC from Table 3.8, the final energy-modified LDC is shown in Figure 3.2. The EENS of the system after base-shaving with Unit#1 is equal to the area below the energy modified LDC:

$$\begin{aligned} \text{EENS}_1 &= 36.22 \cdot 100 + 1.26 \cdot 42.4 + 2.52 \cdot 22.4 + 16.22 \cdot 20 \\ &\quad + 1.26 \cdot 5.6 + 2.52 \cdot 0.6 = 4064.8 \text{ MWh} \end{aligned}$$

The same approach can be applied to base-shave the LDC with Unit#2, except that now the original curve is the energy-modified curve from Figure 3.2. Since Unit#2 only has one state, there is only one additional LDC as shown in Figure 3.3. The possible load levels in

the figure can be read in column 1 in Table 3.9. The duration of the different load levels for the new capacity modified curve can be calculated from Equation (3.5) and are shown in column 5 of Table 3.9.

Table 3.9: Load levels and duration for the capacity-modified curve, modified by Unit#2.

Load	Duration on original LDC	Duration on original LDC reduced by 10MW	Duration on capacity modified curve
60.00	0.6	0	0.0240
57.48	5.6	0	0.2240
56.22	20	0	0.8000
50.00	20	0.6	1.3760
47.48	20	5.6	6.1760
46.22	20	20	20.000
40.00	22.4	20	20.096
37.48	42.4	20	20.896
36.22	100	20	23.200
30.00	100	22.4	25.504
27.48	100	42.4	44.704
26.22	100	100	100.00

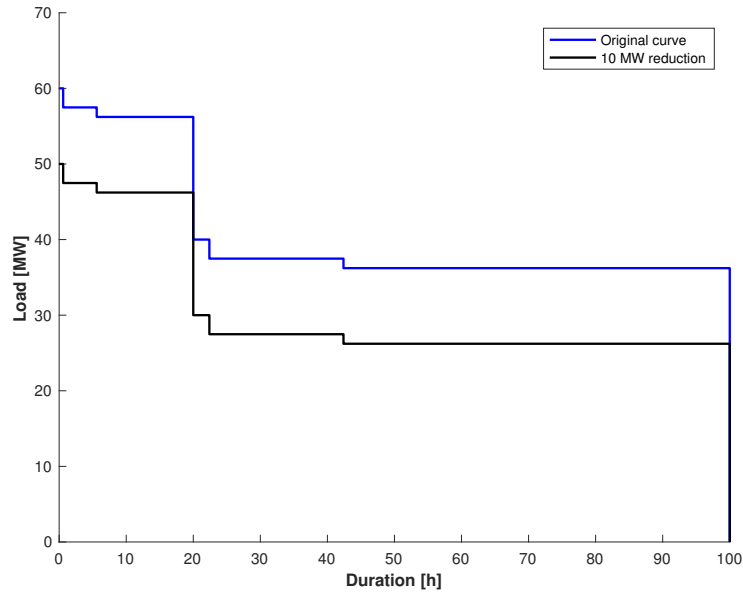


Figure 3.3: Original and 10MW reduction LDC after modification by Unit#2.

The load levels in the new energy-modified curve are calculated as before from Equation (3.6):

$$L_e(1) = 60.00 - [60.00 - 60.00] \cdot \frac{118}{960} = 60.00$$

$$L_e(2) = 60.00 - [60.00 - 57.48] \cdot \frac{118}{960} = 59.69$$

$$L_e(3) = 60.00 - [60.00 - 56.22] \cdot \frac{118}{960} = 59.54$$

$$L_e(4) = 57.48 - [57.48 - 50.00] \cdot \frac{118}{960} = 56.56$$

$$L_e(5) = 57.48 - [57.48 - 47.48] \cdot \frac{118}{960} = 56.25$$

$$L_e(6) = 56.22 - [56.22 - 46.22] \cdot \frac{118}{960} = 54.99$$

$$L_e(7) = 40.00 - [40.00 - 40.00] \cdot \frac{118}{960} = 40.00$$

$$L_e(8) = 40.00 - [40.00 - 37.48] \cdot \frac{118}{960} = 39.69$$

$$L_e(9) = 40.00 - [40.00 - 36.22] \cdot \frac{118}{960} = 39.54$$

$$L_e(10) = 37.48 - [37.48 - 30.00] \cdot \frac{118}{960} = 36.56$$

$$L_e(11) = 37.48 - [37.48 - 27.48] \cdot \frac{118}{960} = 36.25$$

$$L_e(12) = 36.22 - [36.22 - 26.22] \cdot \frac{118}{960} = 34.99$$

Plotting every energy-modified load level with the duration of the capacity-modified LDC from Table 3.9, the final energy-modified LDC is shown in Figure 3.4. The EENS of the system after base-shaving with Unit#2 is equal to the area under the energy modified LDC:

$$\begin{aligned} \text{EENS}_2 &= 34.99 \cdot 100 + 1.26 \cdot 44.704 + 0.31 \cdot 25.504 + 2.98 \cdot 23.2 + 0.15 \cdot 20.896 \\ &+ 0.31 \cdot 20.096 + 14.99 \cdot 20 + 1.26 \cdot 6.176 + 0.31 \cdot 1.376 + 2.98 \cdot 0.8 \\ &+ 0.15 \cdot 0.224 + 0.31 \cdot 0.024 = 3952.2 \text{MWh} \end{aligned}$$

From the two numerical examples, it can be seen that the EENS of the systems is almost the same. The small error is probably due to rounding error in the calculation of the curtailed energy. This means that the capacity-modification method and load-modification method should produce the same reliability indices, which is in accordance with [22].

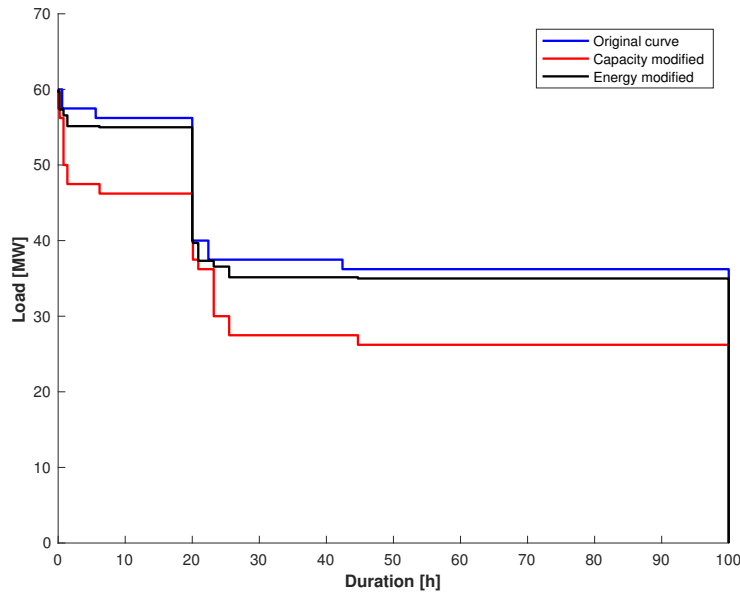


Figure 3.4: Original, capacity modified and energy modified LDC after modification by Unit#2.

### 3.3 The Forced Outage Ratio Modification Method

The FOR modification method for considering energy-limited units is described in [21]. This method incorporates the limitation in energy by looking at the limitation as an equivalent failure. If the unit is considered as energy-limited for generation purposes, that is if the energy required from the unit is larger than the expected energy of the unit, the probability for each generation state is modified.

Assuming the limited-unit is base loaded, the expected period of need for the unit,  $T_e$  is equal to the entire study period,  $T$ . Next, the expected energy of the unit, given in Equation (3.1), is compared to the available energy of the unit, Equation (3.3). Here there are two possibilities:

1. If Expected Energy  $\leq$  Available Energy, the unit is not considered as limited and the probabilities for the generation states remain unchanged.
2. If Expected Energy  $>$  Available Energy, the unit is considered energy-limited and the probabilities for the generation states need to be modified.

If a unit is considered energy-limited, for a multi-state unit, the modified probabilities can be calculated from Equations (3.7)-(3.8):

$$p'_i = \frac{E_i}{C_e \cdot T} \text{ for } i = 1, \dots, N - 1 \quad (3.7)$$

$$p'_0 = 1 - \sum_{i=1}^{N-1} p'_i \quad (3.8)$$

where  $p'_{N-1}$  and  $p'_0$  are the probabilities for the unit being up and down, respectively.  $p'_i$  is the probability for being in a derated state and  $N$  the number of states.  $E_i$  is the energy allocated to state  $i$ , calculated from Equation (3.9), and  $C_e$  is the expected capacity, given by Equation (3.10):

$$E_i = \frac{C_i \cdot p_i}{C_e} \cdot \text{Available Energy} \quad (3.9)$$

$$C_e = \sum_{i=0}^{N-1} C_i \cdot p_i \quad (3.10)$$

For a two-state unit, Equations (3.7)-(3.8) can be reduced to Equations (3.11)-(3.12):

$$p_1' = \frac{\text{Available Energy}}{C_1 \cdot T} \quad (3.11)$$

$$p_0' = 1 - \frac{\text{Available Energy}}{C_1 \cdot T} \quad (3.12)$$

where  $E_i = \text{Available Energy}$ .

### 3.3.1 Numerical Example

The data for the generation system and load model are the same as before and are given in Tables 3.1 - 3.3. The first step is to compare the expected energy of the units to the available energy of the units. This calculation was performed in section 3.1.1, and the results were:

$$\text{Expected Energy}_1 = (0.0 \cdot 0.03 + 10.0 \cdot 0.25 + 15.0 \cdot 0.72) \cdot 100 = 1330 \text{ MWh}$$

$$\text{Available Energy}_1 = (200.0 \cdot 0.3 + 350.0 \cdot 0.5 + 500.0 \cdot 0.2) = 335 \text{ MWh}$$

$$\text{Expected Energy}_2 = (0.0 \cdot 0.04 + 10.0 \cdot 0.96) \cdot 100 = 960 \text{ MWh}$$

$$\text{Available Energy}_2 = (70.0 \cdot 0.4 + 150.0 \cdot 0.6) \cdot 100 = 118 \text{ MWh}$$

From the results it is clear that the expected energy from the units is larger than the available energy, thus the units are considered as energy-limited. The next step is to modify the probabilities of each capacity state.

#### Modifying the probabilities of Unit#1

The first unit considered is Unit#1. This is a multi-state unit, so the probabilities must be modified by Equations (3.7)-(3.8). The expected capacity from Unit#1 is calculated from Equation (3.10) as:

$$C_e = 0 \cdot 0.03 + 10 \cdot 0.25 + 15 \cdot 0.72 = 13.3 \text{ MW}$$

#### State 1

$$E_1 = \frac{C_1 \cdot p_1}{C_e} \cdot \text{Available Energy} = \frac{10 \cdot 0.25}{13.3} \cdot 335 = 62.96992481 \text{ MWh}$$

$$p_1' = \frac{E_1}{C_e \cdot T} = \frac{62.96992481}{13.3 \cdot 100} = 0.04734580813$$

**State 2**

$$E_2 = \frac{C_2 \cdot p_2}{C_e} \cdot \text{Available Energy} = \frac{15 \cdot 0.72}{13.3} \cdot 335 = 272.0300752 \text{ MWh}$$

$$p'_2 = \frac{E_2}{C_e \cdot T} = \frac{272.0300752}{13.3 \cdot 100} = 0.2045338911$$

**State 0**

$$p'_0 = 1 - (p'_1 + p'_2) = 0.7481203008$$

**Modifying the probabilities of Unit#2**

The second unit considered is Unit#2. This is not a multi-state unit, hence the probabilities must be modified by Equations (3.11)-(3.12). The expected capacity from Unit#1 is calculated from Equation (3.10) as:

$$C_e = 0 \cdot 0.04 + 10 \cdot 0.96 = 9.6 \text{ MW}$$

**State 1**

$$E_1 = \frac{C_1 \cdot p_1}{C_e} \cdot \text{Available Energy} = \frac{10 \cdot 0.96}{9.6} \cdot 118 = 118 \text{ MWh}$$

$$p'_1 = \frac{E_1}{C_e \cdot T} = \frac{118}{9.6 \cdot 100} = 0.1229166667$$

**State 0**

$$p'_0 = 1 - p'_1 = 0.8770833333$$

The modified capacity-probability tables for the units are given in Table 3.10.

Table 3.10: FOR modified capacity-probability table for Unit#1 and Unit#2.

<u>Capacity probability Unit#1</u>		<u>Capacity probability Unit#2</u>	
Capacity [MW]	Probability	Capacity [MW]	Probability
0.0	0.74812030080	0	0.87708333333
10.0	0.04734580813	10	0.12291666667
15.0	0.20453389110		

### Calculation of EENS

After the modified probabilities have been obtained, the EENS from this two-unit system can be calculated. Before any of the units are added to the system, there is no generation to serve the load demand. Thus there is a probability of 1.0 of a capacity of 0 MW, and the EENS is equal to the area under the load curve of Table 3.3, shown as the original load duration curve in Figure 3.1.

$$\text{EENS}_0 = 4400 \text{ MWh} \cdot 1.0 = 4400 \text{ MWh}$$

Unit#1 is added first. The COPT after the addition of Unit#1 is given in Table 3.11. By convolving the COPT and the load model (blue curve in Figure 3.1), the EENS for the system at this level is calculated from Equation (2.7):

$$\text{EENS}_1 = 29001 \cdot 0.2045 + 3900 \cdot 0.0473 + 4400 \cdot 0.7481 = 4069.16 \text{ MWh}$$

Table 3.11: System COPT after adding FOR modified Unit#1.

State 'j'	Capacity outage $x_j$ [MW]	Individual probability $p(X = x_j)$	Cumulative probability $P(X \geq x_j)$
1	0	0.2045	1.0
2	10	0.0473	0.7925
3	15	0.7481	0.7481

Next, Unit#2 is added to the system. The updated COPT is given in Table 3.12. Convolving the updated COPT with the load model results in the following EENS:

$$\begin{aligned} \text{EENS}_2 &= 1900 \cdot 0.0251 + 2900 \cdot 0.1853 + 3400 \cdot 0.0919 \\ &\quad + 3900 \cdot 0.0415 + 4400 \cdot 0.6562 = 3946.65 \text{ MWh} \end{aligned}$$

A comparison of the EENS for the different methods is provided in Table 3.13.

Table 3.12: System COPT after adding FOR modified Unit#2.

State 'j'	Capacity outage $x_j$ [MW]	Individual probability $p(X = x_j)$	Cumulative probability $P(X \geq x_j)$
1	0	0.0251	1.0
2	10	0.1853	0.9747
3	15	0.0919	0.7896
4	20	0.0415	0.6977
5	25	0.6562	0.6562

Table 3.13: Comparison of the EENS from the different modification methods

	Capacity modification method	Load modification method	FOR modification method
EENS <sub>1</sub>	4065 MWh	4064.8 MWh	4069.16 MWh
EENS <sub>2</sub>	3947 MWh	3952.2 MWh	3946.65 MWh

As can be seen from Table 3.13, all three methods yield almost identical results. Only the CMM has been tested on the RBTS and the IEEE-RTS, and the results are shown in Chapter 5.



# Chapter 4

## Run-of-the-River in Reliability

### Evaluation

A large part of the thesis work has been devoted to investigate the comprehensive reliability model of a ROR power plant, based on a suitable integration of contents from two different papers from the literature. This chapter presents the details of the integrated methodological approach to identify the effect of ROR units on generation system reliability. Details of the basic ROR reliability modelling that take into account both river inflows and generation unit failures are presented in Section 4.1. The basic ROR model is then extended, as shown in Section 4.2, to additionally take into account the failure rates of all the components of a typical ROR plant (and not just the failure rates of generation units).

#### 4.1 Reliability Evaluation of a Run-of-the-River Power Plant

The main uncertainty regarding the output power of a run-of-the-river power plant (ROR) is due to the inflow of water. The reason for this is that a ROR cannot fully regularize its water usage, as the power plant only has a small or no reservoir at all. Since the water inflows can have a big variation throughout a year and can fluctuate seasonally and regionally, it is important to incorporate this uncertainty in reliability studies. In [27], a model for evaluating ROR generation availability is presented. The model considers the uncertainties of river inflows and generation units' operation. In the following section the method used in

[27] is described and the results are reproduced. By combining a two-state generator Markov model with a multistate river inflow Markov model the reliability of a hydropower plant can be evaluated precisely. The use of the  $k$ -means clustering technique modifies a large amount of river inflow values.

### 4.1.1 River Inflow Model

Due to its random behavior, a river inflow can be modeled as a stochastic process. A stochastic process can be defined as a collection of random variables where each variable is indexed in a mathematical set. In this case, the random variable is the inflow and the index of the process is the time. To analyze the behavior of the river, a Markov chain model is utilized and is shown in Figure 4.1. Each state represents an inflow value, and the transition rate between state  $i$  and state  $j$  is denoted  $\lambda_{ij}$ .

There are a few necessary assumptions that need to be addressed in order to represent a process by a Markov chain. First, the occurrence of the next state only depends on the actual state. Secondly, the process need to be stationary. For a process to be stationary the transition rates between states needs to be constant during the whole process. One of the characteristics of a stationary process is that its mean and standard variation are constant, independently of the sequence of analyzed data [23]. But this is not the case for a wind series according to [29], as seasonal variations leads to the mean and standard variation of a wind series not being constant, hence wind is not a stationary process. As seasonal variations also applies to water inflow, the same can be concluded about a water inflow series. However, this effect can be disregarded if the amount of data is large and over a long time period or the data used does not follow any specific trend of any particular period [30].

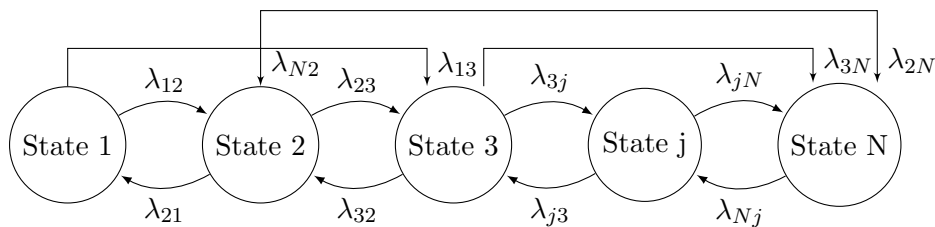


Figure 4.1: Markov model of river inflow, adapted from [27].

Figure 4.2 shows two plots of inflow data obtained from a Brazilian river. Figure 4.2a shows the annual inflow series from the year 1931 to 2004, while Figure 4.2b shows the values in a chronological order. The inflows are the mean inflow for each month and the data are taken from [27]. The way to obtain the Markov model of this river inflow is to obtain all the unique inflow values and calculate the transition rates between them. However, since an annual inflow series contains a lot of different inflow values, the Markov model would be huge and the process of obtaining the transition rates would be time-consuming. A way of reducing the number of inflow states without inducing too much error to the calculation is to use the statistical clustering technique *k*-means [31].

### ***k*-means Clustering Technique**

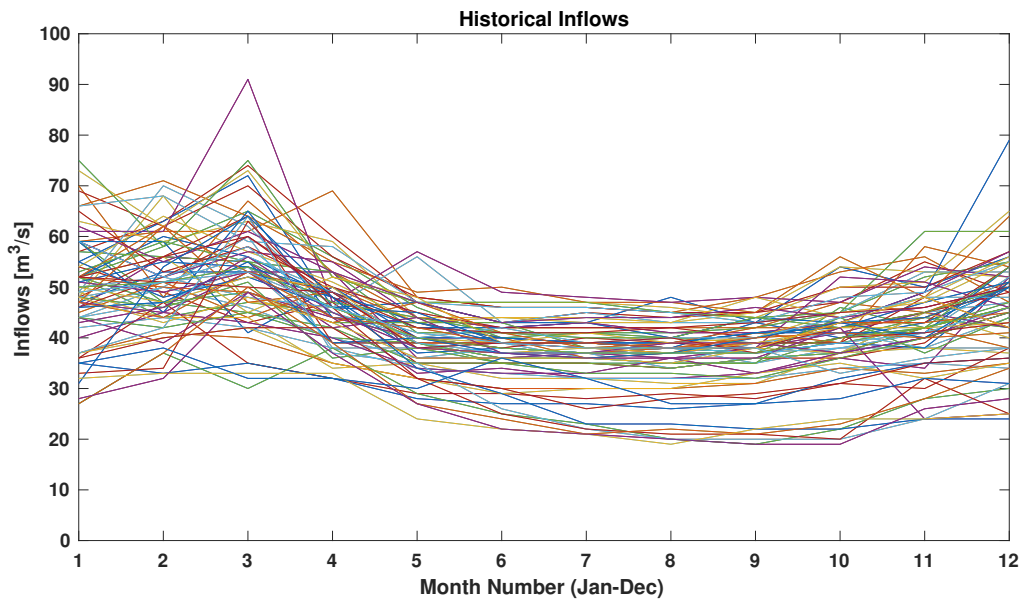
Cluster analysis, or clustering, is used for grouping similar objects and therefore helps to discover distribution of patterns and interesting correlations in large data sets. The objects in the same group have more in common with each other than to the objects in another group. These groups are also called clusters. This form of analysis technique has been in use in a wide variety of fields, such as psychology and other social sciences, biology, statistics, pattern recognition, machine learning and data mining [32]. The technique is also used concerning the electrical power system and power production. In [33], *k*-means is used to estimate 9 characteristic load curves for the electricity system in Karnataka in 1994, which was used to explain sources of variation in hourly demand. In [32], *k*-means is used to determine the availability of micro hydropower in India. In [26], *k*-means is used to cluster wind speed data, although this is a modified method called the *Global Fast k-Means Clustering Algorithm*, which is less dependent on the initial conditions compared to the algorithm described below.

### Clustering Algorithm

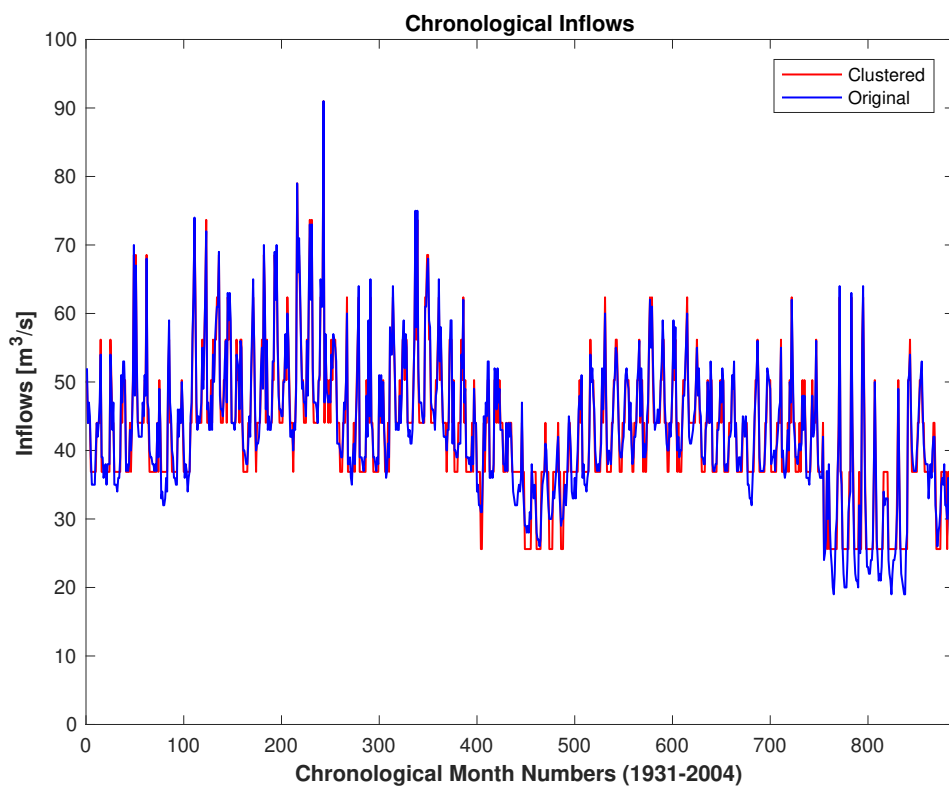
The goal of the k-means clustering algorithm is to divide  $n$  objects into  $k$  clusters, where each object belongs to the cluster with the nearest mean. The algorithm is as follows [34]:

- Input: The number of clusters  $k$ , set of objects  $x_1, \dots, x_n$
1. Place  $k$  centroids  $c_1, \dots, c_k$  at random locations inside the limits of the set of objects  $x_1, \dots, x_n$ 
    - The centroids are the initial cluster means
  2. For the set of objects  $x_1, \dots, x_n$ , calculate the distance from each object  $x_i$  to each centroid  $c_j$  and assign the objects to the cluster with the nearest cluster centroid
    - The distance (Euclidian) is calculated from  $D_{ji} = |c_j - x_i|$
  3. For each cluster  $j = 1, \dots, k$ , calculate the new centroid mean  $c_j$  of all objects  $x_i$  assigned to cluster  $j$  in step 2
    - The new centroid mean is calculated by summing the values of the objects in cluster  $j$  and divide by the number of objects in the cluster
  4. Repeat steps 2 and 3 until convergence, that is when the centroids remain unchanged after an iteration





(a) Annual inflow series (1931-2004).



(b) Chronological inflows (January 1931 - December 2004).

Figure 4.2: Annual and chronological inflows of a Brazilian river (1931-2004), adapted from [27].

To simplify the computation of the river inflow Markov model the number of inflow states is reduced with the  $k$ -means algorithm described above. The number of clusters was chosen as ten in [27] because it was the minimal number of clusters that provided a representative time series. The original inflow series has a total of 888 inflow values, where 59 of those values are unique. After applying the  $k$ -means clustering technique, the 888 inflow values are sorted into ten clusters, where each cluster is associated with one inflow value, i.e. the centroid of the cluster. The centroids of the ten clusters are shown in Table 4.1. The original and the clustered time series are shown in Figure 4.2b. The difference between the clustered inflow and the original inflow are shown in Figure 4.3. It can be observed that most of the difference is in the range of 2-3  $m^3/s$ .

Table 4.1: The cluster centroids produced by the k-means technique.

Cluster (#)	1	2	3	4	5	6	7	8	9	10
Centroid [ $\frac{m^3}{s}$ ]	50.28	25.61	79.00	91.00	62.36	73.67	68.55	44.04	56.18	36.88

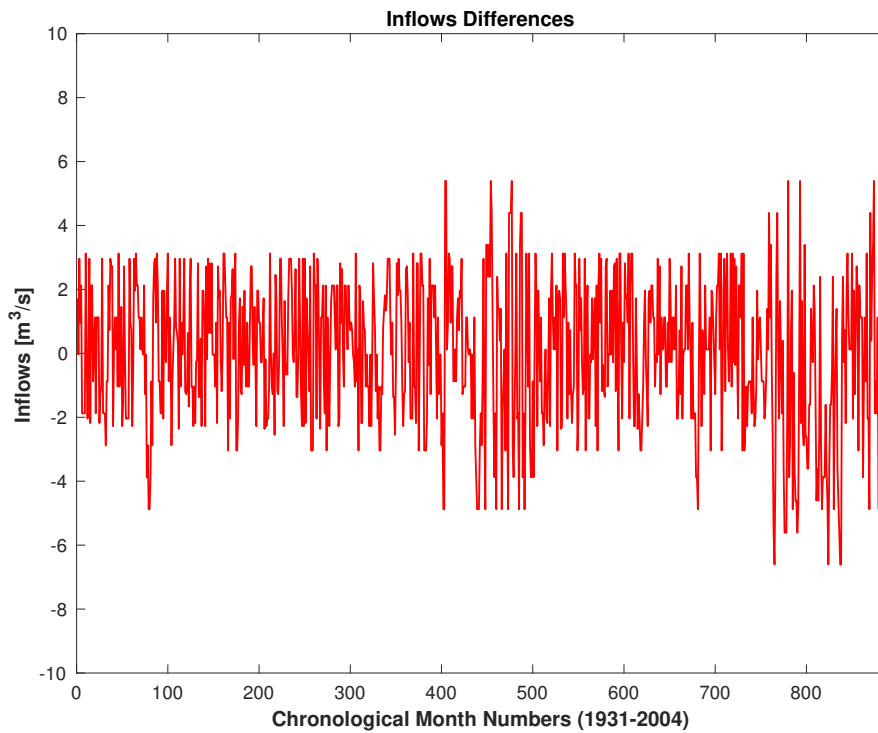


Figure 4.3: Difference between the clustered time series and the original one.

### 4.1.2 Markov Chain Model of the River Inflow

Once the number of inflow states are reduced the Markov model of the river inflow can be obtained. Since ten clusters were used in this example, the Markov model in Figure 4.1 can be updated to include  $N = 10$  states. The Markov model of the clustered river inflow can be seen in Figure 4.4. The transition rates between the clustered states are calculated as follows:

$$\lambda_{ij, i \neq j} = \frac{N_{ij}}{D_i} \tag{4.1}$$

$$\lambda_{ii} = 1 - \sum_{j=1}^n \lambda_{ij, i \neq j} \tag{4.2}$$

where  $\lambda_{ii}$  and  $\lambda_{ij, i \neq j}$  is the transition rate between the diagonal and non-diagonal, respectively, clustered states  $i$  and  $j$ ,  $N_{ij}$  is the number of transitions between states  $i$  and  $j$  and  $D_i$  is the duration of state  $i$ , given by the sum of the  $n$  time intervals in which this state occurs:

$$D_i = \sum_{j=1}^n t_j \tag{4.3}$$

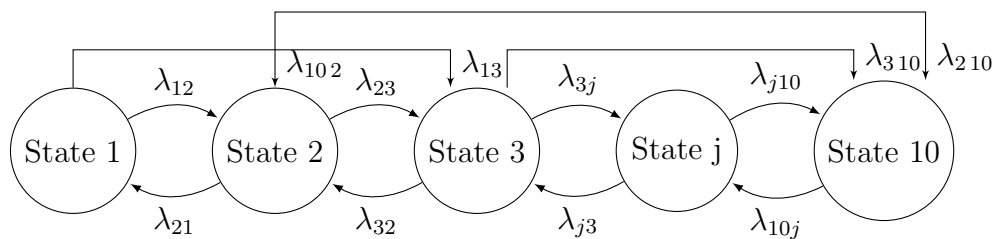


Figure 4.4: Markov model of the clustered river inflow.

#### Small example to demonstrate the transition rates procedure

Consider a time series like the one shown in Figure 4.2b only with a lot fewer inflow values. Let's assume it is adequate to cluster the inflows into three states. If the time series has eight values, an example of a possible clustered chronological inflow order is given in Figure 4.5.

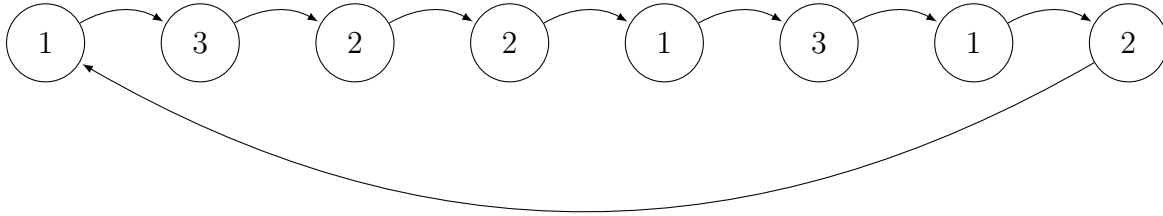


Figure 4.5: An example of a chronological inflow order, clustered into three states.

The first step in obtaining the transition rates is to count the number of transitions from one state to another. So from the sample time series, it can be seen that the transition between State 1 and State 3 occurs two times, between State 2 and State 3 zero times and so on and so forth. The final number of transitions between the states in Figure 4.5 is shown in Table 4.2.

Table 4.2: Number of transitions observed in Figure 4.5.

i/j	1	2	3
1	0	1	2
2	2	1	0
3	1	1	0

The next step in obtaining the transition rates is to calculate the duration of the different states by applying Equation (4.3):

$$D_1 = \sum_{j=1}^3 t_j = 0 + 1 + 2 = 3$$

$$D_2 = \sum_{j=1}^3 t_j = 2 + 1 + 0 = 3$$

$$D_3 = \sum_{j=1}^3 t_j = 1 + 1 + 0 = 2$$

The final step in obtaining the transition rates is to apply Equation (4.1), that is to divide the non-diagonal number of transitions by the durations  $D_1$ ,  $D_2$  and  $D_3$ . The diagonal transition rates are then calculated by Equation (4.2). The final transition rates are given in Table 4.3.

Table 4.3: Transition rates between the states in Figure 4.5.

i/j	1	2	3
1	0	0.333	0.667
2	0.667	0.333	0
3	0.5	0.5	0

■

By following the above described procedure of obtaining the transition rates of a river inflow, the transition rates of the river inflow model can be calculated.

The first step is to calculate the number of transitions between the different inflow states. In Figure 4.6 the first and the last three inflow states of the river inflow time series are shown. By counting all the different transitions, the number of transitions between the clustered inflow states in Figure 4.2b is shown in Table 4.4.

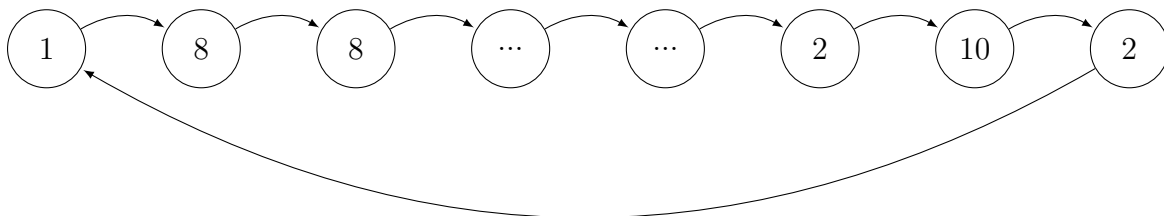


Figure 4.6: The first and last three inflow states of the clustered inflow states in Figure 4.2b.

Table 4.4: Number of transitions between the clustered inflow states in Figure 4.4.

i/j	1	2	3	4	5	6	7	8	9	10
1	36	0	1	0	6	0	5	45	23	14
2	2	70	0	0	0	0	0	0	1	16
3	0	0	0	0	0	0	1	0	0	0
4	0	0	0	0	0	0	0	1	0	0
5	6	0	0	1	4	4	3	5	7	3
6	2	0	0	0	2	0	0	1	1	0
7	3	0	0	0	3	0	2	1	2	0
8	49	1	0	0	5	0	0	135	17	46
9	22	0	0	0	12	2	0	15	13	2
10	10	18	0	0	1	0	0	50	2	217

After the number of transitions is obtained, the duration of the different states can be calculated from Equation (4.3). The transition rates are then obtained by applying Equations (4.1)-(4.2). The results are presented in Table 4.5.

Table 4.5: Transition rates between the clustered inflow states in Figure 4.5.

i/j	1	2	3	4	5	6	7	8	9	10
1	0.2768	0	0.0077	0	0.0462	0	0.0385	0.3462	0.1769	0.1077
2	0.0225	0.7865	0	0	0	0	0	0	0.0112	0.1798
3	0	0	0	0	0	0	1	0	0	0
4	0	0	0	0	0	0	0	1	0	0
5	0.1818	0	0	0.0303	0.1213	0.1212	0.0909	0.1515	0.2121	0.0909
6	0.3333	0	0	0	0.3333	0	0	0.1667	0.1667	0
7	0.2727	0	0	0	0.2727	0	0.1819	0.0909	0.1818	0
8	0.1937	0.0040	0	0	0.0198	0	0	0.5335	0.0672	0.1818
9	0.3333	0	0	0	0.1818	0.0303	0	0.2273	0.1970	0.0303
10	0.0336	0.0604	0	0	0.0034	0	0	0.1678	0.0067	0.7281

### 4.1.3 Small Hydro Plant Generation Model

To investigate the generation from a hydropower plant it is important to both incorporate the effects of the variation of the river inflow and the possibility of a generator failure. A generator can be modeled by a two state Markov model, as shown in Figure 4.7, where  $\lambda$  is the failure rate, and  $\mu$  is the repair rate. In [27], the failure rate and repair rate of the generator are given as 1.8 and 88.2, respectively, both with the unit occurrences per year. From the failure and repair rates, the FOR of the generator be calculated from

$$\text{FOR} = \frac{\lambda}{\lambda + \mu} = \frac{1.8}{1.8 + 88.2} = 0.02 = 2\%$$

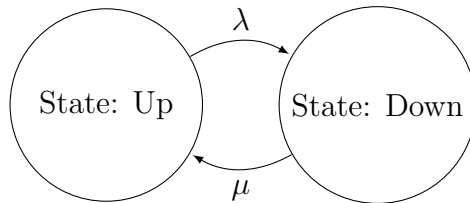


Figure 4.7: Generator model, adapted from [27].

When the generator is in the up-state, the power plant generates power, while when the generator is in the down-state, the power production is zero. The amount of power produced when the generator is in the up-state is given by:

$$P = \gamma \cdot Q \cdot H \cdot \eta_T \cdot \eta_G \quad (4.4)$$

where  $P$  is the power [W],  $\gamma$  is the specific weight of water (9810 [N/m<sup>3</sup>]),  $Q$  is the water inflow [m<sup>3</sup>/s],  $H$  is the water fall height (30 [m]),  $\eta_T$  (80 %) is the turbine efficiency and  $\eta_G$  (80 %) is the generator efficiency. All the values except  $\eta_T$  are taken from [27], where  $\eta_T$  in this example is assumed to be constant, whereas in reality is dependent on the amount of inflow. This will produce a small error compared to the original paper, but won't affect the procedure. By applying Equation (4.4) with the inflow values from Table 4.1 the generated power for each river inflow cluster can be calculated. The results are presented in Table 4.6.

Table 4.6: The cluster centroids and the generated power for each river inflow cluster.

Cluster (#)	1	2	3	4	5	6	7	8	9	10
Centroid [ $\frac{m^3}{s}$ ]	50.28	25.61	79.00	91.00	62.36	73.67	68.55	44.04	56.18	36.88
Power [MW]	15.78	8.04	24.80	28.57	19.58	23.13	21.52	13.82	17.64	11.58

By combining the generator model in Figure 4.7 with the river inflow model in Figure 4.4 the final ROR generation model is produced. Both the generator model and the inflow model are stochastic models, and the transition processes between them are considered as independent events. This means that the up and down states of the generator do not influence the river flow and vice-versa [27]. The inflow and generator models are adequately combined to produce the ROR generation model shown in Figure 4.8. The different clustered inflow states are represented in states 1 to N, while the transitions between them are denoted  $\lambda_{ij}$ . The transitions between the generator up and down states are denoted  $\lambda$  and  $\mu$ . Since the failure of the generator can happen at any moment, every up-state must be linked with a down-state, meaning that the total number of states in the final generation model is N+N states: N up and N down. Since including the generator model has increased the number of states by ten, the transition rates in Table 4.5 has to be updated. The updated transition rates matrix is a 20x20 matrix and is not included in here due to its large size.

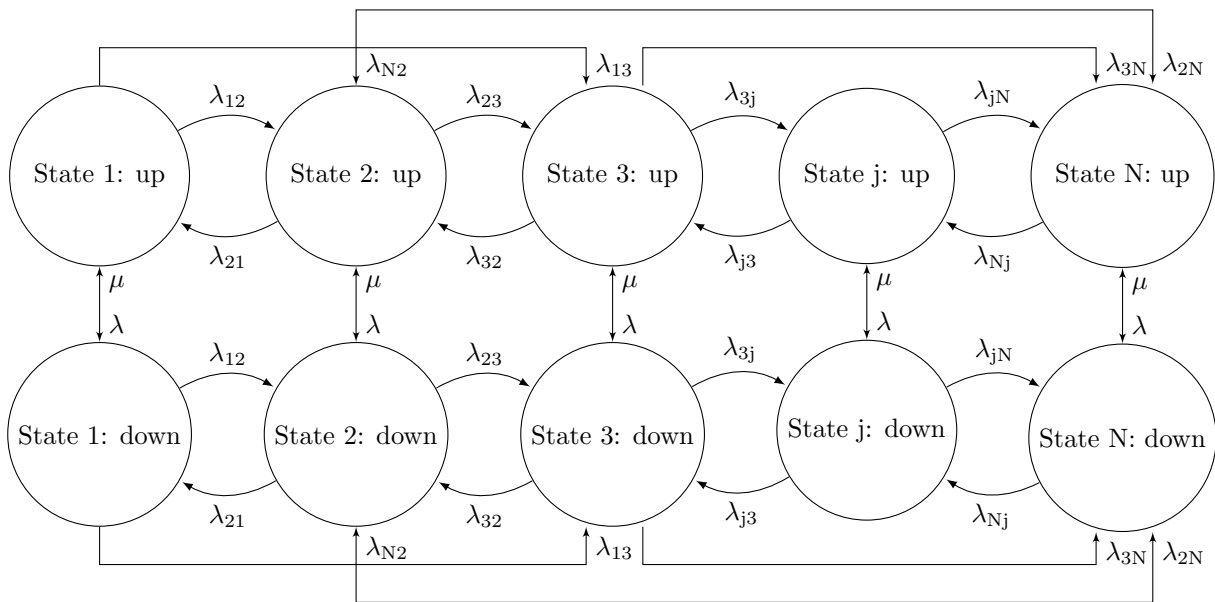


Figure 4.8: ROR generation model with two-state generator model, adapted from [27].

#### 4.1.4 Calculation of the Steady State Probabilities

Once the transition rates are obtained, the steady state probabilities can be calculated from:

$$\mathbf{p}(t)A = \mathbf{0} \quad (4.5)$$

where  $\mathbf{p}(t)$  is the steady state probabilities vector and  $A$  is the transition intensity matrix. The transition rate matrix of the river inflow in Table 4.5 and of the generation system can easily be modified to the transition intensity matrix  $A$  from:

$$a_{ii} = \lambda_{ii} - 1 = - \sum_{j \neq i} \lambda_{ij} \quad (4.6)$$

$$a_{ij} = \lambda_{ij} \quad (4.7)$$

where  $\lambda_{ij}$  is the transition rate from state  $i$  to state  $j$ ,  $\lambda_{ii}$  is the transition rate of the diagonal elements, and  $a_{ii}$  and  $a_{ij}$  is the diagonal and off-diagonal elements in the transition intensity matrix, respectively.

Applying Equations (4.6)-(4.7) the transition intensity matrix of the river inflow is presented in Table 4.7, while the transition intensity matrix of the generation system is left out due to its large size. The steady state probabilities can be obtained by solving Equation (4.5). The procedure for solving Equation (4.5) is by taking the transpose of the equation, producing the general form:

$$\begin{bmatrix} \lambda_{11} & \lambda_{21} & \dots & \lambda_{N1} \\ \lambda_{12} & \lambda_{22} & \dots & \lambda_{N2} \\ \vdots & \vdots & \ddots & \vdots \\ \lambda_{1N} & \lambda_{2N} & \dots & \lambda_{NN} \end{bmatrix} \begin{bmatrix} P_1 \\ P_2 \\ \vdots \\ P_N \end{bmatrix} = \begin{bmatrix} 0 \\ 0 \\ \vdots \\ 0 \end{bmatrix} \quad (4.8)$$

In order to solve Equation (4.8) the full probability condition needs to be applied, that is the sum of all the individual probabilities is equal to one:

$$\left[ P_1 + P_2 + \dots + P_N \right] = 1$$

Therefore, any row in Equation (4.8) can be replaced by this condition, for instance the first row:

$$\begin{bmatrix} 1 & 1 & \dots & 1 \\ \lambda_{12} & \lambda_{22} & \dots & \lambda_{N2} \\ \vdots & \vdots & \ddots & \vdots \\ \lambda_{1N} & \lambda_{2N} & \dots & \lambda_{NN} \end{bmatrix} \begin{bmatrix} P_1 \\ P_2 \\ \vdots \\ P_N \end{bmatrix} = \begin{bmatrix} 1 \\ 0 \\ \vdots \\ 0 \end{bmatrix} \quad (4.9)$$

Equation (4.9) is solved by linear algebra. The results, i.e. the probability of each generation state, is depicted in Tables 4.8 - 4.9. In Table 4.9 the probabilities for all the down states, i.e. zero power produced, are summed together.

Table 4.7: Transition intensity matrix of the river inflow in Figure 4.4.

i/j	1	2	3	4	5	6	7	8	9	10
1	-0.7232	0	0.0077	0	0.0462	0	0.0385	0.3462	0.1769	0.1077
2	0.0225	-0.2135	0	0	0	0	0	0	0.0112	0.1798
3	0	0	-1	0	0	0	1	0	0	0
4	0	0	0	-1	0	0	0	1	0	0
5	0.1818	0	0	0.0303	-0.8787	0.1212	0.0909	0.1515	0.2121	0.0909
6	0.3333	0	0	0	0.3333	-1	0	0.1667	0.1667	0
7	0.2727	0	0	0	0.2727	0	-0.8181	0.0909	0.1818	0
8	0.1937	0.0040	0	0	0.0198	0	0	-0.4665	0.0672	0.1818
9	0.3333	0	0	0	0.1818	0.0303	0	0.2273	-0.8030	0.0303
10	0.0336	0.0604	0	0	0.0034	0	0	0.1678	0.0067	-0.2719

Table 4.8: Probability of generation without considering generator failure.

Power [MW]	Probability (%)	Cumulated probability (%)
8.0385	10.0225	10.0225
11.5761	33.5586	43.5812
13.8249	28.4910	72.0722
15.7829	14.6396	86.7118
17.6366	7.4324	94.1442
19.5772	3.7162	97.8604
21.5178	1.2387	99.0991
23.1254	0.6757	99.7748
24.7997	0.1126	99.8874
28.5667	0.1126	100.0000

Table 4.9: Probability of generation considering generator failure.

Power [MW]	Probability (%)	Cumulated probability (%)
0.0000	2.0000	2.0000
8.0385	9.8221	11.8219
11.5761	32.8874	44.7093
13.8249	27.9212	72.6305
15.7829	14.3468	86.9773
17.6366	7.2838	94.2611
19.5772	3.6419	97.9030
21.5178	1.2140	99.1170
23.1254	0.6622	99.7792
24.7997	0.1104	99.8896
28.5667	0.1104	100.0000

### 4.1.5 Calculation of the Reliability Indices

The energy reliability indices used in this example are, considering IP as the installed power [MW]:

- IE (installed energy) [MWh] - Amount of installed energy in one year, obtained by multiplying IP by 8760 [h].
- EAE (expected available energy) - Amount of energy that can be generated in one year without considering the failure of the generators [MWh].
- EGE (expected generated energy) - Amount of energy that can be generated in one year, considering the failure of the generators [MWh].
- FC (capacity factor) - Obtained by dividing EAE by IE (only considers energy source).
- GAF (generation availability factor) - Obtained by dividing EGE by IE (considers both energy source and generator).

The installed power  $IP = 30$  MW which means the installed energy  $IE = 262\,800$  MWh. Table 4.10 contains the reliability indices calculated for the power plant.

Table 4.10: Reliability indices of the SHPP generation model.

EAE	117 919 MWh
EGE	115 561 MWh
FC	0.44870
GAF	0.43973

## 4.2 Expansion of the ROR Hydro Plant Model

In the previous section, it was shown that due to the variability in the inflow of water, the power output from a ROR unit varies. Even though the combination of the  $k$ -means clustering technique for a Markov river inflow model and a generator model is a powerful technique, it is possible to get an even better solution by also including the other various components in a ROR power plant and not merely the generator. By doing this, the simple two-state generator model used earlier can be replaced by a multi-state ROR power plant model, taking

into account the failure and repair rates of the different components in the ROR power plant. The following section describes a method for constructing a ROR power plant model, and by combining the ROR model with a river inflow model it is possible to obtain precise reliability indices. The method used for constructing the ROR power plant model is adapted from [28]. As it was not possible to obtain the river inflow values used in [28], the river inflow values from Section 4.1 are applied also in this section.

### 4.2.1 Structure of a Typical ROR Power Plant

The structure of a typical ROR power plant and the different components are depicted in Figure 4.9. Some of the water from the river deviates into a forebay tank through a water channel. From the forebay tank, the water is led to the turbine by one or more pipes named penstocks. There is a filter in front of the penstocks to sort out unwanted objects, and at the end of the penstocks is the main valve connected to control the water flow. The water that flows out of the penstocks drives a turbine which is connected to an electrical generator, producing electricity which is transferred to the AC grid through a transformer. The water is then led back to the river or to a lower power plant by the tailrace. If there is too much water in the river or the power plant is shut down due to some error, the water in the forebay tank is then led back to the river by the shoot.

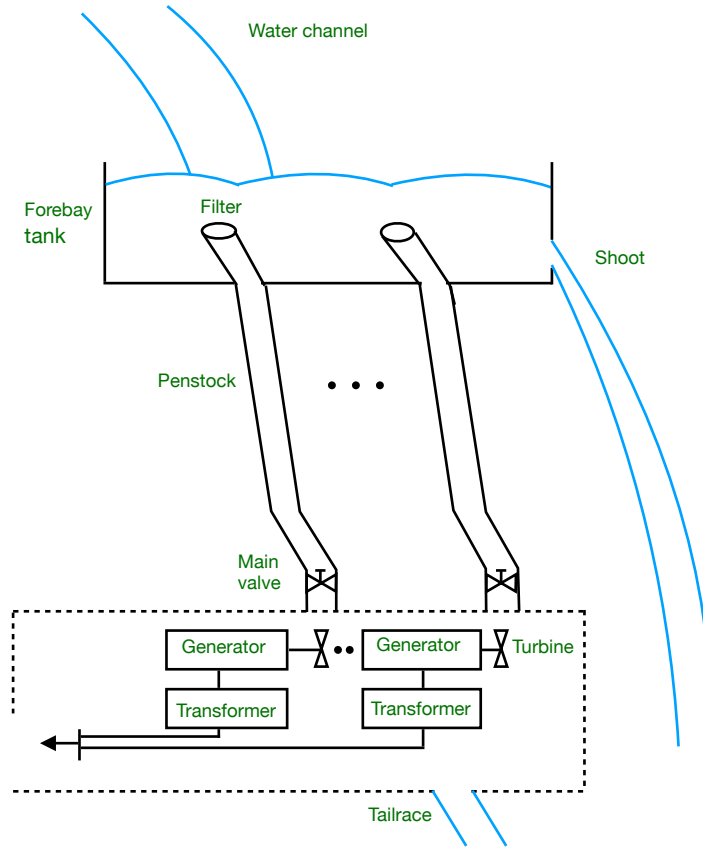


Figure 4.9: Structure of a typical ROR power plant, adapted from [28].

#### 4.2.2 Two-State Markov Model of the ROR Components

As a ROR power plant consists of many different components, successful operation from the power plant is dependent on the successful operation of all the various components. However, successful operation can't be expected forever as each component at any time may fail, making the failure of the components stochastic. The components are also repairable, making the ROR system repairable. Applying the Markov chain technique is a powerful way to understand the probability of events in a ROR power plant. The components are considered to have constant failure and repair rate, meaning that the exponential distribution describes them [35]. The components are either working or not so the two-state Markov model for the generator in Figure 4.7 can be updated to work for all the components in the ROR power plant. The updated Markov model is depicted in Figure 4.10, where  $\lambda_c$  is the failure

rate and  $\mu_c$  is the repair rate for the different components.

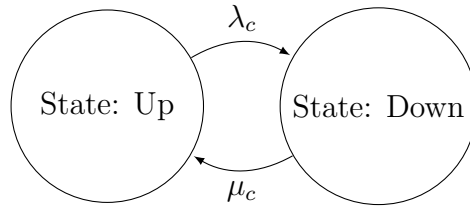


Figure 4.10: Two-state Markov model of ROR power plant components, adapted from [28].

### 4.2.3 Markov Model of ROR Power Plant With One Penstock

By combining the models of the different components, a Markov model of the ROR power plant is constructed. All the relevant states in which the system can inhabit and the transition rates between them should be included. At first, only one penstock is considered, which means that failure of one of the components will lead to an outage of the whole power plant. Thus all the components are in a series configuration from a reliability point of view [28]. The ROR power plant block diagram with one penstock is depicted in Figure 4.11 where the numbers are associated with the components as follows:

1. Water Channel
2. Forebay tank
3. Filter
4. Penstock
5. Main valve
6. Turbine
7. Generator
8. Transformer

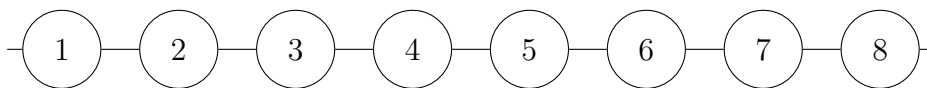


Figure 4.11: Reliability block diagram of a ROR unit with one penstock, adapted from [28].

Since the components are in series and the failure of one component leads to failure of the whole system, then the state-space diagram of the ROR power plant will be similar to the two-state Markov model in Figure 4.11. The failure rate  $\lambda_c$  and repair rate  $\mu_c$  will, in this case, be changed to  $\lambda_{eq}$  and  $\mu_{eq}$  due to the series connection and are calculated as follows for  $n$ -series components [6]:

$$\lambda_{eq} = \sum_{i=1}^n \lambda_i \quad (4.10)$$

$$U_{eq} = \sum_{i=1}^n U_i = \sum_{i=1}^n \lambda_i r_i \quad (4.11)$$

$$r_{eq} = \frac{U_{eq}}{\lambda_{eq}} \quad (4.12)$$

$$\mu_{eq} = \frac{1}{r_{eq}} \quad (4.13)$$

where  $\lambda_i$ ,  $U_i$ , and  $r_i$  is the failure rate, unavailability, and repair time of component  $i$ , respectively.

#### 4.2.4 Markov model of ROR Power Plant With Several Penstocks

Since a ROR power plant may contain several penstocks an updated reliability block diagram is shown in Figure 4.12. The water channel and forebay tank are left out of the parallel connection since the ROR power plant only contains one of each.

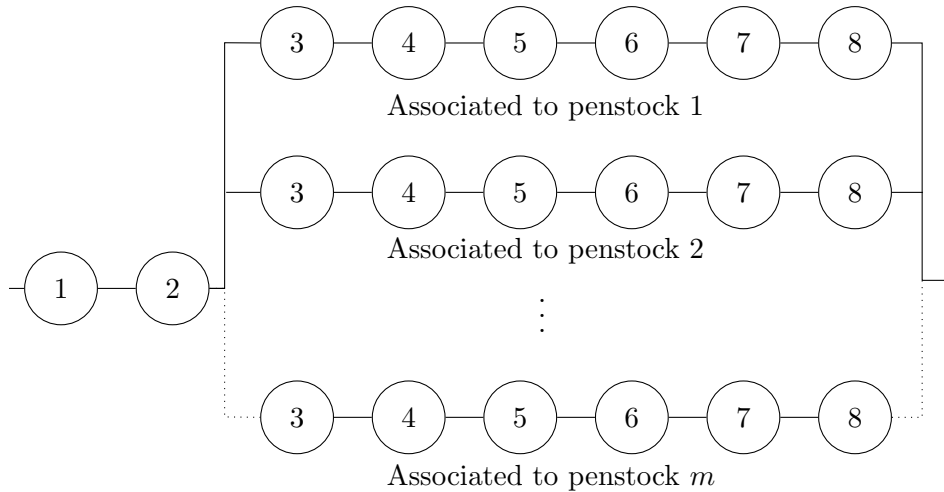


Figure 4.12: Reliability block diagram of a ROR power plant with  $m$  penstocks, adapted from [28].

If the rated power at nominal water flow is  $C$  for each turbine-generator set, any failure of one of the parallel connections in Figure 4.12, that is, failure of either the filter, penstock, main valve, turbine, generator or transformer, would mean that the power plant produces less than its rated power. So the power plant may experience different capacities, called derated states, depending on the failure of the different components. The Markov model of the ROR power plant with several penstocks, without considering the failure of the water channel and forebay tank, is depicted in Figure 4.13.

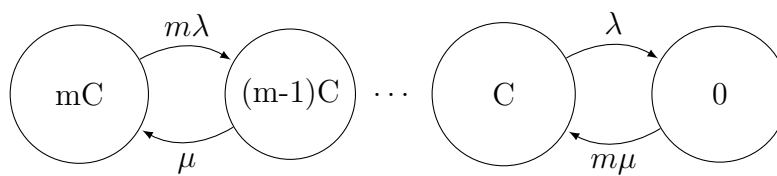


Figure 4.13: Markov model of ROR power plant with  $m$  penstocks without considering the failure of the water channel and forebay tank.

The ROR power plant is dependent on the water channel and forebay tank to produce power. A failure of either would mean an outage of the whole power plant, and thus zero power would be produced. Considering the failure of the water channel and forebay tank leads to the Markov model in Figure 4.14, expanding the Markov model from Figure 4.13, where  $\lambda_a$  and  $\mu_a$  are the equivalent failure and repair rates, respectively, of the water channel

and forebay tank.  $\lambda$  and  $\mu$  are the equivalent failure and repair rates of the penstock series connection, respectively.

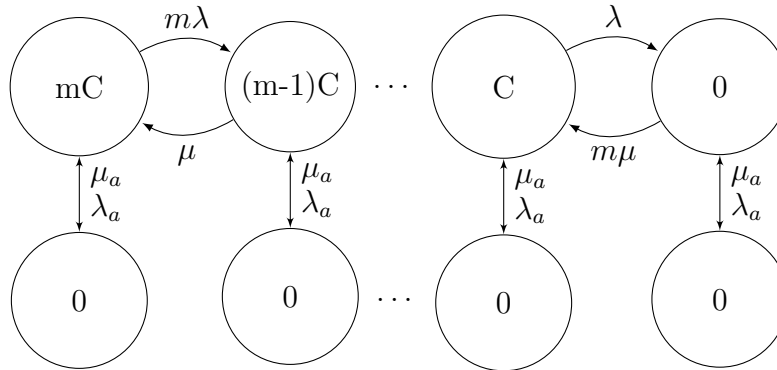


Figure 4.14: Markov model of ROR power plant with  $m$  penstocks considering the failure of the water channel and forebay tank, adapted from [28].

#### 4.2.5 Final Markov Model of ROR Power Plant

In periods where the water level in the river is too extensive, some of the water must be diverted around the power plant. This is made possible by the shoot, which from the reliability point of view acts as a standby element [28]. The power produced from the ROR power plant is transferred to the electrical grid through a power transformer. The final reliability block diagram including both shoot and power transformer is depicted in Figure 4.15. The shoot and power transformer are denoted in the figure as 9 and 10, respectively.

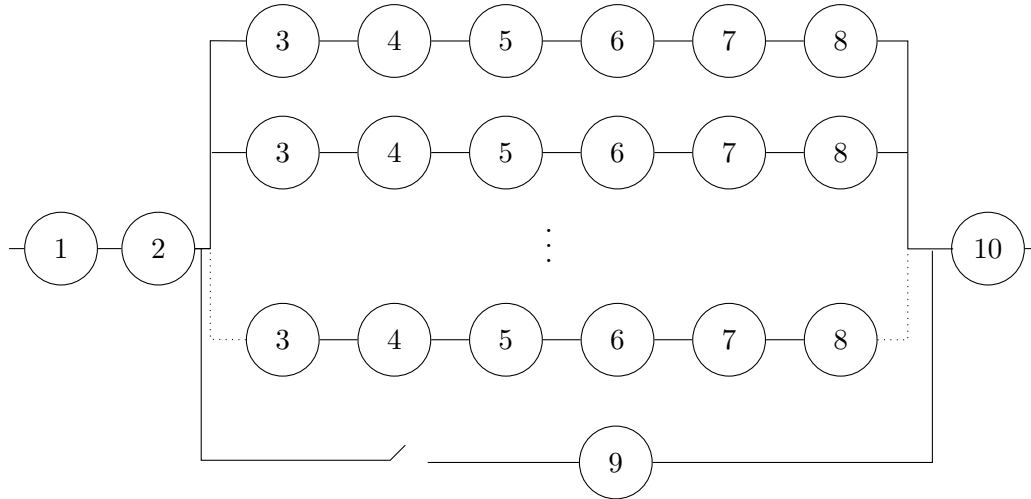


Figure 4.15: Final reliability block diagram of ROR power plant with  $m$  penstocks including shoot and power transformer, adapted from [28].

According to [28], the failure rates of the water channel, forebay tank, penstock, and shoot are so low that they can be ignored in the reliability model without inducing a significant error. Thus in the final Markov model, the equivalent failure and repair rates of the series connection between the water channel and forebay tank are switched to the failure and repair rate of the power transformer. The failure of the power transformer means the connection to the grid is lost, which means zero power production. The final Markov model is depicted in Figure 4.16 where the failure and repair rates of the power transformer are denoted  $\lambda_{tr}$  and  $\mu_{tr}$  respectively.

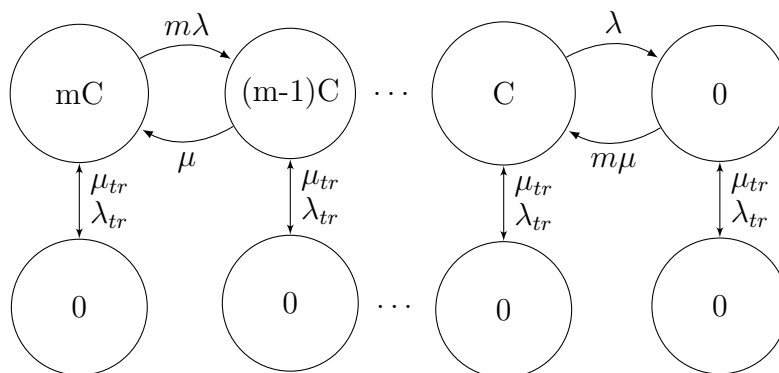


Figure 4.16: Final Markov model of the ROR power plant with  $m$  penstocks considering the failure of the power transformer, adapted from [28].

### 4.2.6 Combining the ROR Power Plant Model With a River Inflow Model

In Section 4.1 a two-state generator model was combined with a ten-state river inflow model, producing the twenty-state generation model shown in Figure 4.8. This generation model can be updated; instead of using the two-state generator model, the ROR power plant model obtained above can be used. Depending on the number of penstocks, the ROR power plant model can either be a two-state or a multi-state model.

By combining the same clustered river inflow values as in Section 4.1 with a ROR power plant model with three penstocks, the extensive ROR Markov model in Figure 4.17 is produced. The columns are associated with different inflow values, while the rows are associated with different power production capacities. That is, in the first row, states 1 to 10, all the penstocks are working, in the second row one penstock has failed, in the third row two penstocks have failed and in the last row either all the penstocks have failed or the power transformer has failed.

### 4.2.7 Calculation of the Steady State Probabilities

Before the steady state probabilities of the ROR model can be obtained all the transition, repair and failure rates in the ROR model in Figure 4.17 must be decided. The transition rates between the different inflow states are the same as before since the same river inflow values are used. In Table 4.11 the failure and repair rates for the different ROR power plant components are listed, adapted from [28]. The equivalent failure and repair rates of the series connection is calculated from Equations (4.10)-(4.13) as follows:

$$\lambda = \sum_{i=1}^n \lambda_i = 2 + 0 + 0.5 + 0.5 + 0.2 + 0.2 = 3.4 \left[ \frac{\text{occurrences}}{\text{year}} \right]$$

$$\mu = \frac{1}{r} = \frac{1}{\frac{2 \cdot 10 + 2 \cdot (0.5 \cdot 87.6) + 2 \cdot (0.2 \cdot 175.2)}{3.4}} \cdot 8760 = 173.54 \left[ \frac{\text{occurrences}}{\text{year}} \right]$$

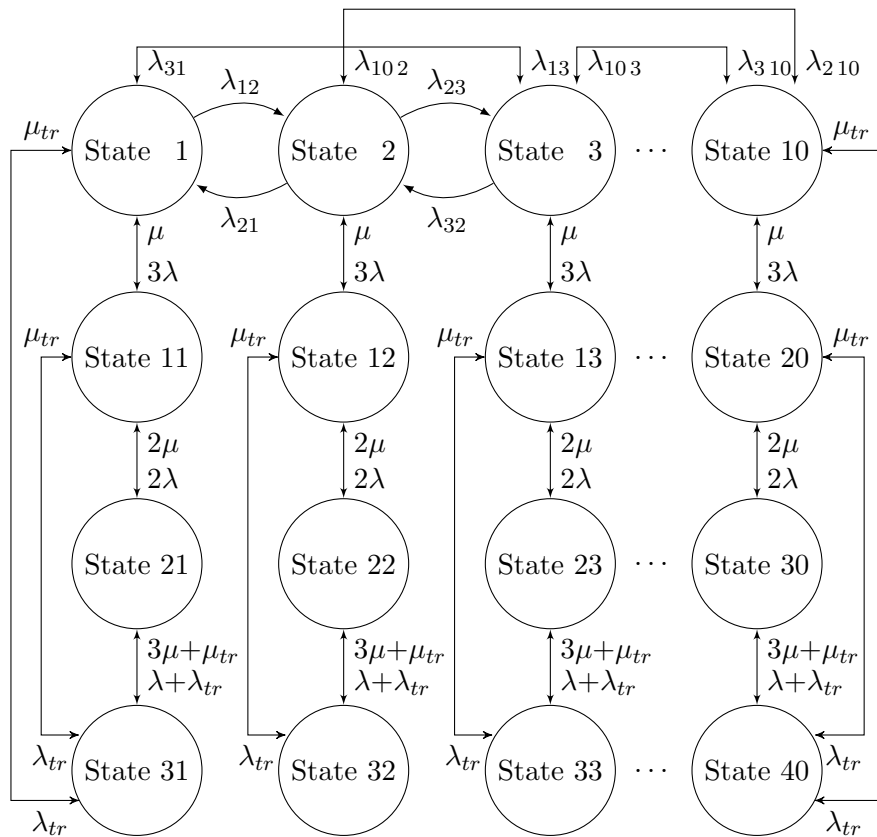


Figure 4.17: Markov model of the combined ROR power plant model and clustered river inflow model. There are transitions between the first and last row for all the columns, but the arrows are left out due to space shortage. The same applies to the transitions between the different columns.

Table 4.11: Reliability data of the ROR power-plant components, adapted from [28].

Components	Component #	Average failure rate [f/year]	Average repair time [h]
Water channel	1	0	-
Forebay tank	2	0	-
Filter	3	2	10
Penstock	4	0	-
Main valve	5	0.5	87.6
Turbine	6	0.5	87.6
Generator	7	0.2	175.2
Transformer	8	0.2	175.2
Shoot	9	0	-
Power transformer	10	0.1	175.2

The probability of the different generation states are calculated in the same way as in Section 4.1, and the results are presented in Table 4.12. All the down states are summed to one, which means the final amount of generation states is 31. The EGE from the ROR power plant is 115 598 MWh which is a bit more than from the hydro model in Section 4.1 which was an EGE of 115 561 MWh. It is difficult to put too much weight on this comparison, as the two examples use different failure and repair rates.

Table 4.12: Probability of generation from the ROR power plant.

Capacity (MW)	Probability	Capacity (MW)	Probability	Capacity (MW)	Probability
0	1.5588E-4	8.0385	0.0945	15.7829	0.1380
2.6795	1.6218E-4	8.2666	1.8222E-6	16.5331	6.5829E-5
3.8587	5.4302E-4	9.2166	0.0159	17.6366	0.0701
4.6083	4.6102E-4	9.5222	1.8222E-6	19.0445	6.5829E-5
5.2610	2.3689E-4	10.5220	0.0082	19.5772	0.0350
5.3590	0.0056	11.5761	0.3163	21.5178	0.0117
5.8789	1.2027E-4	11.7577	0.0042	23.1254	0.0064
6.5257	6.0133E-5	13.0515	0.0021	24.7997	0.0011
7.1726	2.0044E-5	13.8249	0.2686	28.5667	0.0011
7.7085	1.0933E-5	14.3452	0.0070		
7.7174	0.0188	15.4170	0.0004		



# Chapter 5

## Case Study: Utilizing the Methods in Test Systems

In this chapter, two of the methods described in Chapters 3 and 4 for incorporating energy-limited units are applied to the test systems Roy Billinton Test System (RBTS) and IEEE Reliability Test system (IEEE-RTS). The methods are the CMM and the ROR method. The CMM is preferred over the FOR modification method and LMM due to its simplicity. For the ROR power plant, river inflow data from Solbergfoss in the river Glomma in Norway is used.

### 5.1 Test Systems

#### 5.1.1 RBTS

The RBTS is a more practical test system than for instance the IEEE Reliability Test System (IEEE-RTS) [36]. Although the IEEE-RTS is widely used in literature, it may not be perfectly suited for educational purposes due to its large power network. The objective in designing the RBTS was to [37] ”*make it sufficiently small to permit the conduct of a large number of reliability studies with reasonable solution time but sufficiently detailed to reflect the actual complexities involved in a practical reliability analysis*”.

#### Generation data

The installed capacity in the RBTS is 240 MW. The generation system consists of 2x5, 4x20

and 1x40 MW hydro units and 1x10, 1x20 and 2x40 MW thermal units. Generation unit data is shown in Table 5.1. Detailed information about the hydro units in the RBTS is shown in Table 5.2. The capacity and probability of the hydro units are taken from [37] while the energy distribution are taken from [15]. The capacity modified hydro units in the RBTS is shown in Table 5.3, where the capacities are modified by the procedure described in Section 3.1.

Table 5.1: Generating unit reliability data for RBTS, adapted from [37].

Unit size (MW)	Type	Number of units	Forced outage rate
5	hydro	2	0.01
10	thermal	1	0.02
20	hydro	4	0.015
20	thermal	1	0.025
40	hydro	1	0.02
40	thermal	2	0.03

Table 5.2: Capacity probability table for the hydro units in RBTS, adapted from [22].

<u>Capacity probability</u>		<u>Energy distribution</u>	
Capacity [MW]	Probability	Energy [MWh]	Probability
Hydro unit: 2x5 MW			
5.0	0.99	20 000	0.3
0	0.01	16 949	0.4
		14 999	0.3
Hydro unit: 4x20 MW			
20	0.985	80 000	0.3
0	0.015	67 796	0.4
		59 997	0.3
Hydro unit: 1x40 MW			
40	0.98	160 000	0.3
0	0.02	135 593	0.4
		119 994	0.3

Table 5.3: Capacity modified hydro units in RBTS.

Capacity [MW]	Probability
Hydro unit: 2x5 MW	
0	0.01
1.992528	0.99
Hydro unit: 4x20 MW	
0	0.015
8.010280	0.985
Hydro unit: 1x40 MW	
0	0.02
16.102344	0.98

### Load data

The annual peak load for the RBTS is 185 MW. The load data is depicted in Tables B.1-B.3 in Appendix B and is taken from [36]. The data for the weekly peak load is given in percent of the annual peak load, the data for the daily peak load is given in percent of the weekly peak load and the data for the hourly peak load are given in percent of the daily peak load. These values are the same for the RBTS as for the IEEE-RTS [36]. In Figure 2.5 the chronological load levels and the LDC for hourly, daily, weekly and year peak loads are depicted. The load data is a forecast based on previous experience that tries to predict typical yearly and daily load patterns.

### 5.1.2 IEEE-RTS

The IEEE-RTS is designed to do the same studies as the RBTS, but with a much larger generation and load. The installed capacity is 3405 MW, more than ten times larger than that of the RBTS. The IEEE-RTS uses the same load data as the RBTS, only with a peak load of 2850 MW. The generation unit data is shown in Table 5.4. Detailed information about the hydro units in the RBTS is shown in Table 5.5. The capacities and availabilities of the hydro units are taken from [37] while the energy distribution is taken from [15]. The capacity modified hydro units in the RBTS are shown in Table 5.6, where the procedure described in Section 3.1 modifies the capacities.

Table 5.4: Generating unit reliability data for IEEE-RTS, adapted from [36].

Unit size (MW)	Number of units	Forced outage rate
12	5	0.02
20	4	0.10
50	6	0.01
76	4	0.02
100	3	0.04
155	4	0.04
197	3	0.05
350	1	0.08
400	2	0.12

Table 5.5: Capacity probability table for the hydro units in IEEE-RTS, adapted from [22].

<u>Capacity probability</u>		<u>Energy distribution</u>	
Capacity [MW]	Probability	Energy [MWh]	Probability
Hydro unit: 6x50 MW			
50	0.99	200 000	0.3
0	0.01	169 491	0.4
		149 992	0.3

Table 5.6: Capacity modified hydro units in IEEE-RTS.

Capacity [MW]	Probability
Hydro unit: 6x50 MW	
0	0.01
19.924629	0.99

## 5.2 Solbergfoss ROR Power Plant

To test the impact from a ROR power plant on the reliability performance of power systems, data from a Norwegian river is obtained and combined with a ROR power plant model. The river inflow data is provided by Norges vassdrags- og energidirektorat (NVE) and is taken from Solbergfoss in the river Glomma. There are two ROR hydro plants in Solbergfoss: Solbergfoss I and Solbergfoss II. Solbergfoss I was built in 1924, consists of 12 generators with an IC of 108 MW and absorption capacity of 680 m<sup>3</sup>/s. Solbergfoss II was built in 1985, consists of 1 generator with an IC of 100 MW and absorption capacity of 550 m<sup>3</sup>/s. Both power plants exploit a drop of 21 m [38].

The river inflow values are clustered into ten states from the procedure described in Section 4.1. A modified version of the Solbergfoss I power plant is used, with three generators instead of 12. The reliability data of the power plant components are taken from Table 4.11 and is not obtained from Solbergfoss. The clustered river inflow centroids are depicted in Table 5.7. The power output from the ROR power plant is calculated from Equation (4.4),

with a combined generator-turbine efficiency  $\eta = 0.8$ , drop  $H = 21$  m, water density  $\gamma = 1000$  kg/m<sup>3</sup> and water inflow  $Q$  taken from Table 5.7. It is not possible for the power plant to absorb more than 680 m<sup>3</sup>/s, so for all the values larger than this, the remaining water is not used for power production. The generation states and the probability of generation from the modified Solbergfoss power plant are depicted in Table 5.8.

Table 5.7: The cluster centroids produced by the k-means technique for Solbergfoss.

Cluster (#)	1	2	3	4	5	6	7	8	9	10
Centroid [ $\frac{m^3}{s}$ ]	1989.3	647.4	1132.2	1705.8	2389.3	2771.0	1383.6	263.9	441.3	898.2

Table 5.8: Probability of generation from Solbergfoss power plant.

Capacity (MW)	Probability	Capacity (MW)	Probability	Capacity (MW)	Probability
0	1.5588E-4	35.7084	7.0214E-4	72.7220	0.2862
14.4979	2.6126E-4	43.4936	0.1841	106.6887	0.1617
24.2407	4.0630E-4	48.4813	0.0170	107.1252	0.3106
28.9957	0.0109	71.1258	0.0096		
35.5629	2.2956E-4	71.4168	0.0146		

## 5.3 Adequacy Evaluation

In this section, the influence on reliability from energy-limited hydro units in the RBTS and the IEEE-RTS is thoroughly investigated. The CMM is applied and a ROR power plant with Norwegian river inflow values are added to the test systems.

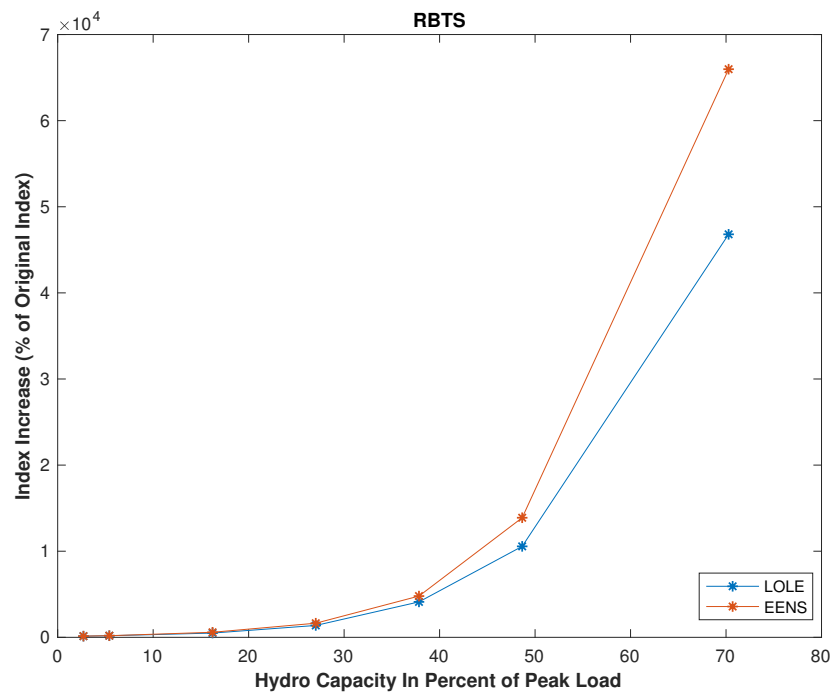
### 5.3.1 Reliability Indices for the RBTS

By convolving the COPT for the capacity modified generation units with the load model, the LOLE and EENS for the system are obtained from MATLAB scripts provided by the Department of Electric Power Engineering at NTNU. The indices are shown in Table 5.9. As the results show, there is a large increase in LOLE and EENS with an increasing amount of

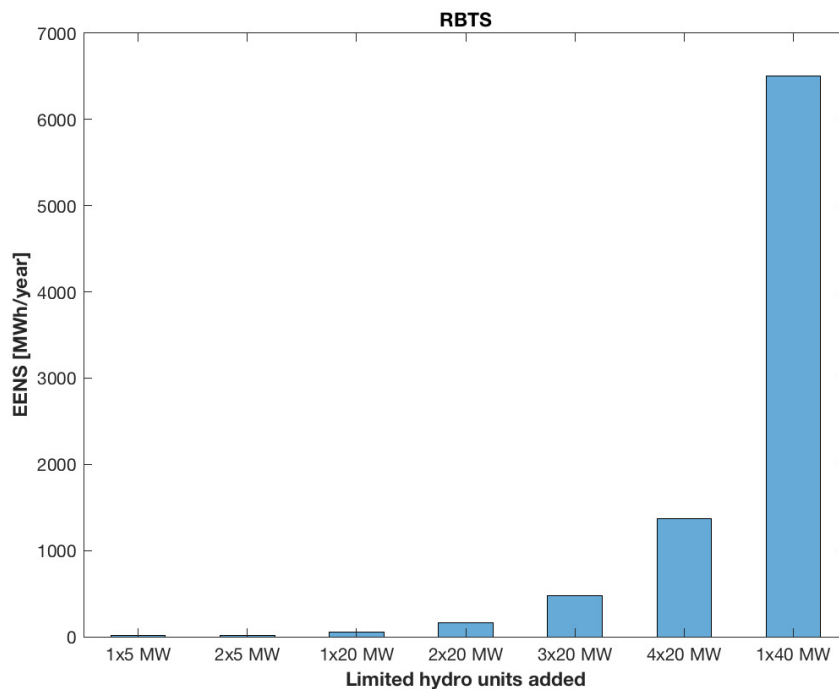
energy limited units. In Figure 5.1 the findings are clarified with the percentage increase in indices compared to the original RBTS for different unit considerations and the increase in EENS for every addition of an energy limited unit. It is clear that the limitations in energy have a significant impact on the system reliability, thus the energy limitations should be considered in a reliability evaluation.

Table 5.9: LOLE and EENS with energy-limited units for the RBTS.

Limited units	Capacity modified LOLE [h/year]	Capacity modified EENS [MWh/year]
None	1.0917	9.8629
1x5 MW	1.4739	13.6508
2x5 MW	2.0282	18.7936
2x5 + 1x20 MW	5.3984	57.9230
2x5 + 2x20 MW	15.0565	161.6408
2x5 + 3x20 MW	45.8064	472.5414
2x5 + 4x20 MW	115.3298	1369.7
2x5 + 4x20 + 1x40 MW	510.9269	6507.0



(a) The index increase with increase in limited hydro capacity for the RBTS.



(b) The EENS increase with each limited hydro unit for the RBTS.

Figure 5.1: The effect limited hydro units have on the reliability indices in the RBTS.

To test the impact from the ROR power plant, three different cases are considered:

1. The original RBTS
2. The original RBTS plus a 27 MW ROR power plant
3. The original RBTS plus a 27 MW conventional unit with a FOR of 4%

The ROR power plant used is the same as discussed in Section 5.2, only with 1/4th of the capacity due to its large size compared to the other RBTS units. The three cases are tested for different peak loads, and the results are shown in Table 5.10. In Figure 5.2 the EENS is plotted for the different peak loads. The addition of a ROR power plant makes the system reliability better, but not as much as a conventional unit. However, the differences are not that large, mainly due to the large river inflow values at Solbergfoss.

Table 5.10: LOLE and EENS for different peak loads.

Peak load	Case 1		Case 2		Case 3	
	LOLE	EENS	LOLE	EENS	LOLE	EENS
170	0.2551	2.1877	0.0308	0.2542	0.0207	0.1674
175	0.4125	3.6583	0.0505	0.4283	0.0345	0.2875
180	0.6940	6.0130	0.0865	0.7149	0.0595	0.4877
185	1.0917	9.8629	0.1376	1.1962	0.0914	0.8108
190	1.7103	15.7897	0.2322	1.9859	0.1498	1.3269
195	2.5187	24.8869	0.3743	3.2894	0.2375	2.1498
200	3.8111	37.9375	0.5975	5.3733	0.3803	3.4550
205	5.3542	57.2021	0.9355	8.6682	0.5782	5.5345
210	7.5889	84.9962	1.3899	13.6861	0.9077	8.7325
215	12.0589	126.5896	2.0753	21.2454	1.4082	13.7382
220	17.2376	188.7735	3.1688	32.4551	2.1044	21.3448
225	25.2192	279.2273	4.6965	49.1818	3.1638	32.6819
230	36.3673	411.9738	6.9248	74.0871	4.6627	49.7404

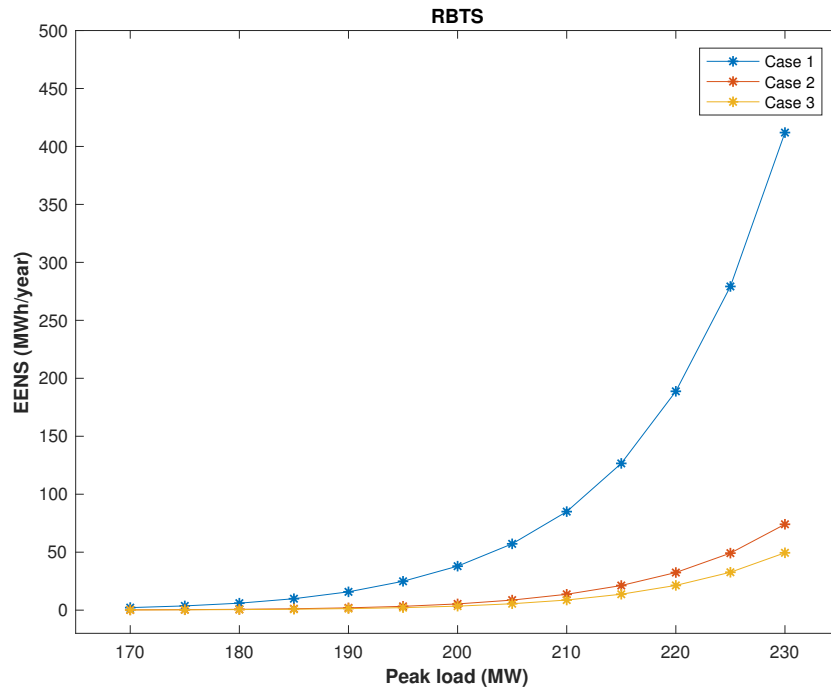


Figure 5.2: EENS for three cases of the RBTS.

### 5.3.2 Reliability Indices for the IEEE-RTS

The LOLE and EENS when modifying the capacity for the hydro units in the IEEE-RTS are shown in Table 5.11. Figure 5.3 shows the index increase with the increase of limited hydro capacity and the increase in EENS when adding energy limited units. The percentage increase in the indices is much more constant for the IEEE-RTS case than for the RBTS case. This is because the RBTS has more hydro units compared to the total IC than the IEEE-RTS. The increase in EENS for each addition of a limited hydro unit is also apparent in this case.

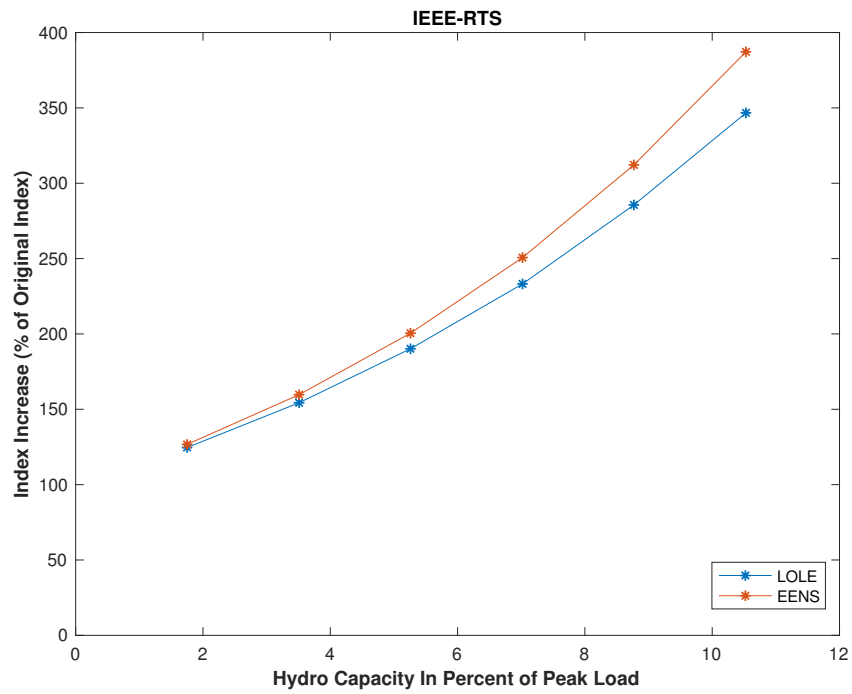
Table 5.11: LOLE and EENS with energy-limited units for the IEEE-RTS.

Limited units	Capacity modified	
	LOLE [h/year]	EENS [MWh/year]
None	9.4192	1176.4
1x50 MW	11.7376	1490.4
2x50 MW	14.5371	1878.7
3x50 MW	17.9118	2358.5
4x50 MW	21.9657	2948.9
5x50 MW	26.9014	3672.2
6x50 MW	32.6542	4554.9

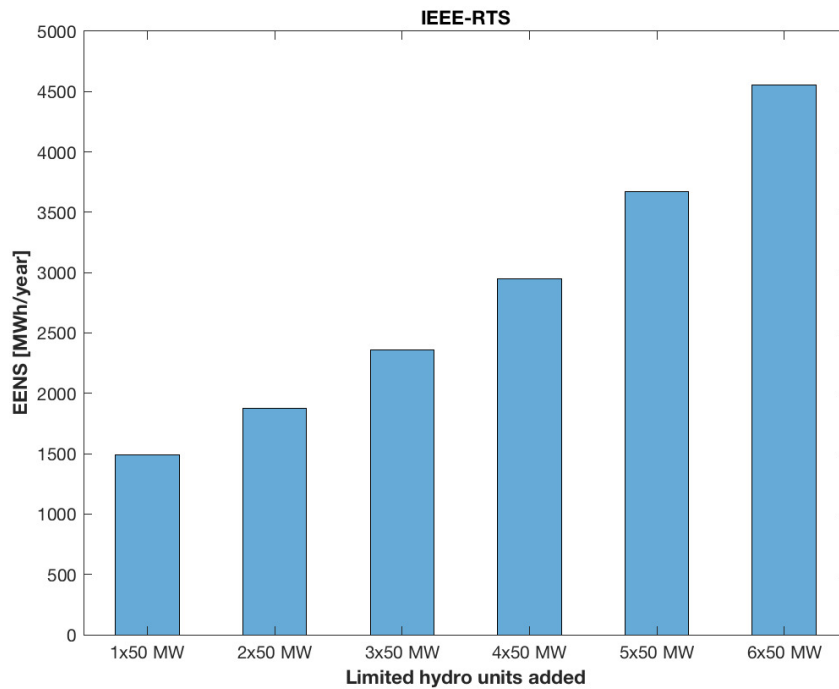
The complete Solbergfoss ROR power plant is added to the IEEE-RTS to test the impact on the system reliability. The LOLE and EENS for different cases are shown in Table 5.12. As the results show, the conventional unit provides better reliability than the ROR plant. This means that to get the same reliability results as a conventional unit, a larger ROR unit must be added.

Table 5.12: Impact on LOLE and EENS in the IEEE-RTS from Solbergfoss ROR.

Description	LOLE [h/year]	EENS [MWh/year]
Original case (OC)	9.4192	1176.4
OC + 1x108 MW conventional	4.3212	505.1455
OC + 2x108 MW conventional	1.8856	206.1265
OC + 1x108 MW ROR	5.0728	598.3960
OC + 2x108 MW ROR	2.6255	295.2286



(a) The index increase with increase in limited hydro capacity for the IEEE-RTS.



(b) The EENS increase with each limited hydro unit for the IEEE-RTS.

Figure 5.3: The effect limited hydro units have on the reliability indices in the IEEE-RTS.

# Chapter 6

## Conclusions and Future Work

### 6.1 Discussion and Conclusions

Reliability studies are an essential part of power system planning and operation studies. A wide range of reliability indices is used by system planner and operators to ensure successful operation of power systems against random failures both in the planning and operational horizons. In generation system reliability studies, it is usual to consider the energy source for generation as always available. This implies that unavailability of generation is solely on account of a generation unit of the power plant. In the case of hydro generation, if the reservoir is sufficiently large enough to guarantee the availability of energy, through a constant regime of inflows, that modelling is correct [39]. However, stochastic nature of inflows and reservoir limitations make hydro generation energy-limited.

This thesis has examined multiple methods for incorporating energy-limited hydro generation units in generation system reliability studies. Three of the methods have focused on hydro generation units with reservoir limitations. The CMM treats the limited hydro units as non-limited, but with a reduced capacity depending on the COPT and the energy distribution of the unit. That the energy-limited hydro units can be treated as non-limited makes the method suitable for use in a test system, as the units can be implemented in the same way as any other conventional unit. The LMM makes use of the energy-limited units to reduce the LDC, and with the remaining non-limited units creates a COPT for calculating the reliability indices. When there are few energy-limited units involved, this method is straightforward and produces accurate results. However, as the number of energy-limited units increases,

the number of load steps may quickly get so large that the method becomes cumbersome. The huge number of load steps may also increase the possibility of making errors. The FOR modification method treats the limited energy of a unit as an equivalent failure, modifying the probabilities for the different generation states from the energy distribution of the unit. This method, as was the case with the CMM, treats the limited units as non-limited, which makes the method easy to implement in a test system.

The CMM was applied to the RBTS and the IEEE-RTS. As the reliability indices in Chapter 5 show, the energy-limited hydro units play a significant role on the system reliability. The increase in EENS with the addition of more energy-limited units is greater for the RBTS than the IEEE-RTS, as Figures 5.1 and 5.3 show. This is because the amount of hydro in the RBTS is much greater than that in the IEEE-RTS, where 54.17% of the IC in the RBTS is hydro compared to 8.81% for the IEEE-RTS.

In addition to these three methods, a large part of the thesis work has been devoted to investigate a comprehensive reliability model of a ROR power plant; this was based on a suitable integration of contents from two different papers from the literature. Two parts of the ROR power plant which cause uncertainty in regards of the power output have been combined to produce this model. Firstly, a river inflow model is obtained. Electric power output from a ROR unit fluctuates as the water flow varies throughout a year. These fluctuations may not be that considerable in the short term, however, for the long term, the water flow varies greatly with the seasonal changes. This may cause great impacts on the system reliability, especially for systems with high hydropower penetration [40]. River flow data from a Brazilian river and a Norwegian river are utilized. Both sets of data provide great material for statistical work with, respectively, 73 and 115 years of monthly mean inflow values. The  $k$ -means clustering technique is used to reduce the large amount of data into 10 clusters. As the plot of the differences between the original and clustered inflow in Figure 4.3 shows, the clustering technique does not induce a significant error; most of the difference is around  $\pm 3 m^3/s$ . This indicates that the clustering approach is very representative of the real inflow series. With the clustered values, a powerful Markov model of the river inflow is created and the probability of the generation states are obtained.

The failure rates of different components in a ROR power plant have then been taken into account. Each component at any given time may or may not function successfully, and a Markov model is applied to evaluate the reliability. Including all the components in a ROR

power plant leads to a large set of equations to be solved, which may be time consuming. However, if the failure and repair rate data for each component are exact, then the model of the ROR power plant is much more precise than a standard unit with only a FOR.

The extended ROR model used in the test systems RBTS and IEEE-RTS combined the two models of both uncertainties, that is uncertainty in water inflow and component failures. As the reliability indices in Figure 5.2 and Tables 5.10 and 5.12 show, the ROR unit improves the reliability indices significantly. Compared to the OC, with the addition of one ROR unit the LOLE is reduced from 9.4192 to 5.0728 h/year, and the EENS is reduced from 1176.4 to 598.3960 MWh/year. The improvement in the reliability indices is even greater for the conventional unit, which means that if one wants to obtain the same improvement in reliability from a ROR unit as a conventional unit, the capacity of the ROR unit must be larger. This is due to the variability in the river inflow, which in some periods is lower than the absorption capacity of the ROR power plant. However, even though there is variability in the river inflow, the difference in the indices of the ROR unit and the conventional unit are not that large. This is because even though the river flow varies, the flow is larger than the absorption capacity of the power plant most of the time, as shown in Table 5.7.

## 6.2 Improvements and Suggestions for Future Work

A few simplifications were made during the calculations of the ROR power plant generation states. One was that the turbine efficiency was assumed constant for all river inflows, when in fact the efficiency changes a bit depending on the amount of inflow. Also, the number of clustering states was set to 10 for the river inflows used in this thesis. This number was taken from [27], which was based on an analysis of the difference between the clustered states and the original inflow, and the expected reduction of computational effort. There may be a better number of clusters for the Solbergfoss river, but 10 clusters provided sufficient accuracy.

Only one ROR power plant has been used in this thesis, but if a river with several ROR power plants is used, a model of a cascade ROR power plants can be made [28]. A way to improve one of the modification methods is to obtain a more detailed energy distribution.



# Bibliography

- [1] UNFCCC, “Paris Agreement,” *Conference of the Parties on its twenty-first session*, vol. 21932, no. December, p. 32, 2015. [Online]. Available: <https://unfccc.int/process/the-paris-agreement/what-is-the-paris-agreement>
- [2] G. W. E. Council, “Global Wind Report,” 2017. [Online]. Available: <https://gwec.net/publications/global-wind-report-2/>
- [3] J. S. for Policy Report, “PV Status Report,” 2017. [Online]. Available: <http://publications.jrc.ec.europa.eu/repository/bitstream/JRC108105/kjna28817enn.pdf>
- [4] International Hydropower Association, “Hydropower Status Report 2018,” pp. 1–41, 2018. [Online]. Available: <https://www.hydropower.org/publications/2018-hydropower-status-report>
- [5] R. Billinton and R. Allan, “Power-system reliability in perspective,” *Electronics and Power*, vol. 30, no. 3, pp. 231–236, 1984.
- [6] R. Billinton and R. N. Allan, *Reliability Evaluation of Power Systems*, 1996. [Online]. Available: <http://link.springer.com/10.1007/978-1-4899-1860-4>
- [7] K. Koldingsnes, *Reliability-based Derating Approach for Interconnectors*. Masters’ thesis, NTNU, 2017.
- [8] R. Billinton, “Bibliography on the application of probability methods in power system reliability evaluation,” *IEEE Transactions on Power Apparatus and Systems*, vol. PAS-91, no. 2, pp. 649–660, 1972.
- [9] P. S. E. Committee, “Bibliography On The Application Of Probability Methods In Power System Reliability Evaluation 1971-1977,” *IEEE Transactions on Power Apparatus and Systems*, vol. PAS-97, no. 6, pp. 2235–2242, 1978.

- [10] R. N. Allan and R. Billinton, "Bibliography on the Application of Probability Methods in Power System Reliability Evaluation 1977-1982," *IEEE Transactions on Power Apparatus and Systems*, vol. PAS-103, no. 2, pp. 275 – 282, 1984.
- [11] R. N. Allan, R. Billinton, S. Shadidehpour, and C. Singh, "Bibliography on the Application of Probability Methods in Power System Reliability Evaluation 1982-1987," *IEEE Transactions on Power Apparatus and Systems*, vol. 3, no. 4, pp. 1555–1564, 1988.
- [12] R. N. Allan, R. Billinton, A. Breipohl, and C. Grigg, "Bibliography on the Application of Probability Methods in Power System Reliability Evaluation: 1987-1991," *IEEE Transactions on Power Systems*, vol. 9, no. 1, pp. 41–49, 1994.
- [13] R. N. Allan, R. Billinton, A. M. Breipohl, and C. H. Grigg, "Bibliography on the application of probability methods in power system reliability evaluation," *IEEE Transactions on Power Systems*, vol. 14, no. 1, pp. 51–57, 1999.
- [14] R. Billinton, M. Fotuhi-Firuzabad, and L. Bertling, "Bibliography on the Application of Probability Methods in Power System Reliability Evaluation 1996-1999," *IEEE Transactions on Power Systems*, vol. 16, no. 4, pp. 595–602, 2001.
- [15] P. G. Harrington and R. Billinton, "Reliability Evaluation in Energy Limited Generating Capacity Studies," *IEEE Transactions on Power Apparatus and Systems*, vol. PAS-97, no. 6, pp. 2076–2085, 1978.
- [16] C. Singh and Q. Chen, "An analytical technique for the reliability modeling of generation systems including energy limited units," *IEEE Transactions on Power Systems*, vol. 2, no. 1, pp. 123–128, 1987.
- [17] Q. Chen and C. Singh, "Equivalent load method for calculating frequency & duration indices in generation capacity reliability evaluation," *IEEE Transactions on Power Systems*, vol. 1, no. 1, pp. 101–107, 1986.
- [18] R. R. Booth, "Power System Simulation Model Based On Probability Analysis," *IEEE Transactions on Power Apparatus and Systems*, vol. PAS-91, no. 1, pp. 62–69, 1972.
- [19] R. Billinton and L. Cheung, "Load modification: a unified approach for generating-capacity reliability evaluation and production-cost modelling," *IEE Proceedings C Generation, Transmission and Distribution*, vol. 134, no. 4, pp. 273–280, 1987.

- [20] Q. Chen, "A comparative study of power generation system reliability including the consideration of energy limited units," *1991 Third International Conference on Probabilistic Methods Applied to Electric Power Systems*, 1991.
- [21] A. Patton, C. Singh, and M. Sahinoglu, "Operating considerations in generation reliability modeling - an analytical approach," *IEEE Transactions on Power Apparatus and Systems*, vol. PAS-100, no. 5, pp. 2656–2663, 1981.
- [22] B. Bagen, D. Huang, and C. Singh, "A new analytical technique for incorporating base loaded energy limited hydro units in reliability evaluation," *Electric Power Systems Research*, vol. 131, pp. 218–223, 2016.
- [23] A. P. Leite, C. L. T. Borges, and D. M. Falcão, "Probabilistic Wind Farms Generation Model for Reliability Studies Applied to Brazilian Sites," *IEEE Transactions on Power Systems*, vol. 21, no. 4, pp. 1493–1501, 2006.
- [24] T. Manco and A. Testa, "A Markovian Approach to Model Power Availability of a Wind Turbine," *2007 IEEE Lausanne Power Tech*, 2007.
- [25] A. S. Dobakhshari and M. Fotuhi-Firuzabad, "A reliability model of large wind farms for power system adequacy studies," *IEEE Transactions on Energy Conversion*, vol. 24, no. 3, pp. 792–801, 2009.
- [26] Y. Guo, H. Gao, and Q. Wu, "A Combined Reliability Model of VSC-HVDC Connected Offshore Wind Farms Considering Wind Speed Correlation," *IEEE Transactions on Sustainable Energy*, vol. 8, no. 4, pp. 1637–1646, 2017.
- [27] C. L. T. Borges and R. J. Pinto, "Small hydro power plants energy availability modeling for generation reliability evaluation," *IEEE Transactions on Power Systems*, vol. 23, no. 3, pp. 1125–1135, 2008.
- [28] E. Khalilzadeh, M. Fotuhi-Firuzabad, F. Aminifar, and A. Ghaedi, "Reliability modeling of run-of-the-river power plants in power system adequacy studies," *IEEE Transactions on Sustainable Energy*, vol. 5, no. 4, pp. 1278–1286, 2014.
- [29] R. B. Corotis, A. B. Sigl, and J. Klein, "Probability models of wind velocity magnitude and persistence," *Solar Energy*, vol. 20, no. 6, pp. 483–493, 1978.

- [30] G. C. Thomann and M. Barfield, "The time variation of wind speeds and windfarm power output in Kansas," *IEEE Transactions on Energy Conversion*, vol. 3, no. 1, pp. 44–49, 1988.
- [31] W. S. Sarle, A. K. Jain, and R. C. Dubes, *Algorithms for Clustering Data*, 1990, vol. 32, no. 2.
- [32] S. P. Adhau, R. M. Moharil, and P. G. Adhau, "K-Means clustering technique applied to availability of micro hydro power," *Sustainable Energy Technologies and Assessments*, vol. 8, pp. 191–201, 2014.
- [33] P. Balachandra and V. Chandru, "Modelling electricity demand with representative load curves," *Energy*, vol. 24, no. 3, pp. 219–230, 1999.
- [34] J. MacQueen, *Proceedings of the Berkeley Symposium on mathematical Statistics and Probability*, 1967, vol. 1, no. 14.
- [35] R. Billinton and R. N. Allan, *Reliability Evaluation of Engineering Systems*, 2nd ed. Plenum Press, New York, 1992.
- [36] P. M. Subcommittee, "IEEE Reliability Test System," *IEEE Transactions on Power Apparatus and Systems*, vol. PAS-98, no. 6, pp. 2047–2054, 1979. [Online]. Available: <http://ieeexplore.ieee.org/document/4113721/>
- [37] R. Billinton, S. Kumar, N. Chowdhury, K. Chu, K. Debnath, L. Goel, E. Khan, P. Kos, G. Nourbakhsh, and J. Oteng-Adjei, "A reliability test system for educational purposes - basic data," *IEEE Transactions on Power Systems*, vol. 4, no. 3, pp. 1238–1244, 1989.
- [38] NVE, "Kraftverk: Solbergfoss," 2015. [Online]. Available: <https://www.nve.no/vann-vassdrag-og-miljo/nves-utvalgte-kulturminner/kraftverk/solbergfoss/>
- [39] R. Allan and R. Billinton, "Probabilistic assessment of power systems," *Proceedings of the IEEE*, vol. 88, no. 2, pp. 140–162, 2000.
- [40] L. Chen, Y. Ding, H. Li, and G. Jin, "Long-term reliability evaluation for small hydro-power generations based on flow runoff theory," *The Journal of Engineering*, vol. 2017, no. 13, pp. 1708–1712, 2017.

# Appendix A

## Example of the Recursive COPT Algorithm

A generation system consists of three equal two-state generators, with capacity = 100 MW and FOR = 0.1. The information is provided in Table A.1.

Table A.1: Generation system data for recursive COPT procedure..

Generator	Capacity [MW]	FOR
1	100	0.1
2	100	0.1
3	100	0.1

### Adding unit 1

Since there is no entries in the COPT yet, Equation (2.3) is used to initialize the values. From Equation (2.2) we get:

$$P^{new}(X \geq 0) = (1 - p_{down}) \cdot P^{old}(X \geq 0) + p_{down} \cdot P^{old}(X \geq 0 - 100)$$

$$P^{new}(X \geq 0) = (1 - 0.1) \cdot 1 + 0.1 \cdot 1 = 1$$

$$P^{new}(X \geq 100) = (1 - p_{down}) \cdot P^{old}(X \geq 100) + p_{down} \cdot P^{old}(X \geq 100 - 100)$$

$$P^{new}(X \geq 100) = (1 - 0.1) \cdot 0 + 0.1 \cdot 1 = 0.1$$

Thus the COPT after addition of unit number 1 is given in Table A.2.

Table A.2: COPT after addition of unit 1

State 'j'	Capacity outage $x_j$ [MW]	Individual probability $p(X = x_j)$	Cumulative probability $P(X \geq x_j)$
1	0	0.9	1.0
2	100	0.1	0.1

**Adding unit 2**

$$P^{new}(X \geq 0) = (1 - p_{down}) \cdot P^{old}(X \geq 0) + p_{down} \cdot P^{old}(X \geq 0 - 100)$$

$$P^{new}(X \geq 0) = (1 - 0.1) \cdot 1 + 0.1 \cdot 1 = 1$$

$$P^{new}(X \geq 100) = (1 - p_{down}) \cdot P^{old}(X \geq 100) + p_{down} \cdot P^{old}(X \geq 100 - 100)$$

$$P^{new}(X \geq 100) = (1 - 0.1) \cdot 0.1 + 0.1 \cdot 1 = 0.19$$

$$P^{new}(X \geq 200) = (1 - p_{down}) \cdot P^{old}(X \geq 200) + p_{down} \cdot P^{old}(X \geq 200 - 100)$$

$$P^{new}(X \geq 200) = (1 - 0.1) \cdot 0 + 0.1 \cdot 0.1 = 0.01$$

Thus the updated COPT after addition of unit number 2 is given in Table A.3.

Table A.3: COPT after addition of unit 2

State 'j'	Capacity outage $x_j$ [MW]	Individual probability $p(X = x_j)$	Cumulative probability $P(X \geq x_j)$
1	0	0.81	1.0
2	100	0.18	0.19
3	200	0.01	0.01

**Adding unit 3**

$$P^{new}(X \geq 0) = (1 - p_{down}) \cdot P^{old}(X \geq 0) + p_{down} \cdot P^{old}(X \geq 0 - 100)$$

$$P^{new}(X \geq 0) = (1 - 0.1) \cdot 1 + 0.1 \cdot 1 = 1$$

$$P^{new}(X \geq 100) = (1 - p_{down}) \cdot P^{old}(X \geq 100) + p_{down} \cdot P^{old}(X \geq 100 - 100)$$

$$P^{new}(X \geq 100) = (1 - 0.1) \cdot 0.19 + 0.1 \cdot 1 = 0.271$$

$$P^{new}(X \geq 200) = (1 - p_{down}) \cdot P^{old}(X \geq 200) + p_{down} \cdot P^{old}(X \geq 200 - 100)$$

$$P^{new}(X \geq 200) = (1 - 0.1) \cdot 0.01 + 0.1 \cdot 0.19 = 0.028$$

$$P^{new}(X \geq 300) = (1 - p_{down}) \cdot P^{old}(X \geq 300) + p_{down} \cdot P^{old}(X \geq 300 - 100)$$

$$P^{new}(X \geq 300) = (1 - 0.1) \cdot 0 + 0.1 \cdot 0.01 = 0.001$$

Thus the final updated COPT after addition of unit number 2 is given in Table A.4.

Table A.4: COPT after addition of unit 3

State 'j'	Capacity outage $x_j$ [MW]	Individual probability $p(X = x_j)$	Cumulative probability $P(X \geq x_j)$
1	0	0.729	1.0
2	100	0.243	0.271
3	200	0.027	0.028
4	300	0.001	0.001



# Appendix B

## Load Data for the Test Systems

Table B.1: Daily load data.

Day	Daily Peak Load (DPL)
'd'	[% of Weekly Peak Load] (WPL)
1	93
2	100
3	98
4	96
5	94
6	77
7	75

Table B.2: Weekly load data.

Week	WPL	Week	WPL	Week	WPL	Week	WPL
'w'	[% of YPL]						
1	86.2	14	75.0	27	75.5	40	72.4
2	90.0	15	72.1	28	81.6	41	74.3
3	87.8	16	80.0	29	80.1	42	74.4
4	83.4	17	75.4	30	88.0	43	80.0
5	88.0	18	83.7	31	72.2	44	88.1
6	84.1	19	87.0	32	77.6	45	88.5
7	83.2	20	88.0	33	80.0	46	90.9
8	80.6	21	85.6	34	72.9	47	94.0
9	74.0	22	81.1	35	72.6	48	89.0
10	73.7	23	90.0	36	70.5	49	94.2
11	71.5	24	88.7	37	78.0	50	97.0
12	72.7	25	89.6	38	69.5	51	100.0
13	70.4	26	86.1	39	72.4	52	95.2

Table B.3: Hourly load data.

Hour 'h'	Winter weeks	Winter	Summer weeks	Summer	Spring/Fall weeks	Spring/Fall
	1-8&44-52	1-8&44-52	18-30	18-30	9-17&31-43	9-17&31-43
	Weekday	Weekend	Weekday	Weekend	Weekday	Weekend
	[% of DPL]	[% of DPL]	[% of DPL]	[% of DPL]	[% of DPL]	[% of DPL]
1	67	78	64	74	63	75
2	63	72	60	70	62	73
3	60	68	58	66	60	69
4	59	66	56	65	58	66
5	59	64	56	64	59	65
6	60	65	58	62	65	65
7	74	66	64	62	72	68
8	86	70	76	66	83	74
9	95	80	87	81	95	83
10	96	88	95	86	99	89
11	96	90	99	91	100	92
12	95	91	100	93	99	94
13	95	90	99	93	93	91
14	95	88	100	92	92	90
15	93	87	100	91	90	90
16	94	87	97	91	88	86
17	99	91	96	92	90	85
18	100	100	96	94	92	88
19	100	99	93	95	96	92
20	96	97	92	95	98	100
21	91	94	92	100	96	97
22	83	92	93	93	90	95
23	73	87	87	88	80	90
24	63	81	72	80	70	85



# Appendix C

## Brazilian River Inflow Data

Table C.1: Monthly mean inflow values of Brazilian river ( $m^3/s$ ), adapted from [27].

Year/month	1	2	3	4	5	6	7	8	9	10	11	12
1931	52	44	47	45	39	35	35	35	35	40	44	42
1932	44	47	54	39	39	36	37	38	35	38	38	38
1933	54	49	43	47	35	35	35	34	36	36	39	51
1934	47	53	53	48	37	38	37	38	43	40	43	50
1935	70	48	67	53	44	42	42	42	42	47	45	51
1936	48	68	47	46	40	39	39	38	38	37	38	37
1937	44	39	49	44	33	34	32	32	33	36	34	52
1938	59	47	45	40	39	36	36	35	35	46	42	46
1939	44	50	46	40	36	38	37	34	36	37	45	47
1940	57	63	74	60	47	43	45	44	45	47	55	49
1941	55	63	72	46	47	43	43	48	43	54	50	56
1942	59	61	61	69	48	46	46	45	48	53	56	47
1943	63	59	63	59	44	44	44	43	45	54	53	52
1944	46	56	55	44	40	40	39	38	38	41	45	42
1945	52	58	65	56	46	40	41	41	42	45	52	55

Table C.2: Continued monthly mean inflow values of Brazilian river ( $m^3/s$ ).

Year/month	1	2	3	4	5	6	7	8	9	10	11	12
1946	49	70	62	46	56	43	45	43	43	45	53	53
1947	69	62	70	56	48	46	46	45	45	50	50	57
1948	52	60	56	48	42	42	43	40	44	43	49	79
1949	66	71	64	55	49	50	47	47	45	56	48	64
1950	73	62	73	52	47	47	47	46	44	50	51	65
1951	61	61	91	47	57	49	48	47	48	47	54	52
1952	57	56	55	53	41	41	41	40	39	39	42	47
1953	46	50	60	38	38	39	36	35	39	41	38	44
1954	48	56	64	39	39	39	38	37	39	39	48	42
1955	59	45	65	44	43	39	39	38	37	39	38	51
1956	45	51	44	50	43	40	36	37	41	39	58	54
1957	54	64	57	51	43	44	43	43	48	44	48	56
1958	59	52	57	55	44	42	43	41	41	43	49	57
1959	75	58	75	52	47	47	47	45	44	45	61	61
1960	66	68	59	58	47	46	46	45	43	48	49	55
1961	65	53	58	50	45	42	42	42	40	43	43	54
1962	59	59	41	50	40	40	39	39	41	41	41	54
1963	52	62	47	49	39	39	39	38	39	37	42	38
1964	49	44	44	34	35	32	32	31	31	37	45	40
1965	47	45	53	53	36	36	37	36	38	52	51	46
1966	52	47	49	43	43	43	38	38	37	44	37	44
1967	42	44	42	38	34	33	32	32	32	34	35	34
1968	36	47	35	32	29	29	28	29	28	31	30	38
1969	35	33	35	32	28	27	27	26	27	32	35	36

Table C.3: Continued monthly mean inflow values of Brazilian river ( $m^3/s$ ).

Year/month	1	2	3	4	5	6	7	8	9	10	11	12
1970	37	41	40	35	32	30	30	30	31	34	33	35
1971	37	40	42	35	32	29	30	30	33	35	32	35
1972	40	45	43	40	34	33	33	36	33	37	40	46
1973	48	46	51	36	38	35	35	34	36	37	42	54
1974	50	52	48	46	40	38	37	38	37	39	41	52
1975	46	52	60	48	40	38	40	39	38	42	45	49
1976	51	55	54	49	43	40	39	39	41	42	47	51
1977	52	50	49	43	47	41	38	39	42	42	44	50
1978	52	56	45	52	48	39	41	39	40	45	47	55
1979	62	55	61	53	47	43	44	44	46	44	46	50
1980	53	59	55	47	44	41	40	40	44	42	45	50
1981	59	52	58	45	40	42	39	40	40	44	48	48
1982	52	56	60	49	42	41	41	42	43	45	46	50
1983	55	48	52	46	45	39	39	38	38	43	44	50
1984	47	44	53	49	38	37	37	38	38	43	43	45
1985	50	47	52	50	38	37	38	37	39	42	42	43
1986	51	49	53	42	44	37	37	39	39	37	40	45
1987	44	42	45	42	35	35	33	33	32	36	40	45
1988	48	51	56	49	39	37	37	37	37	38	41	46
1989	52	51	50	49	38	39	39	40	37	40	41	43
1990	46	47	55	39	40	37	36	37	40	43	40	50
1991	47	62	53	44	42	39	39	38	40	41	40	41
1992	48	43	48	43	36	36	36	35	38	43	48	42
1993	43	46	56	45	38	37	36	36	36	42	24	25

Table C.4: Continued monthly mean inflow values of Brazilian river ( $m^3/s$ ).

Year/month	1	2	3	4	5	6	7	8	9	10	11	12
1994	27	37	30	38	29	25	23	20	19	22	28	30
1995	37	42	64	37	35	26	22	20	20	20	24	31
1996	33	34	63	46	32	25	22	21	21	20	32	25
1997	31	54	64	48	34	29	23	23	22	22	24	24
1998	27	37	50	39	27	24	21	22	21	23	28	34
1999	32	33	33	33	24	22	21	19	22	24	24	25
2000	28	32	49	37	27	22	21	20	19	19	26	28
2001	50	51	54	46	40	38	37	37	37	40	42	46
2002	49	51	53	46	41	39	38	38	38	33	36	38
2003	36	40	42	42	32	30	26	28	29	31	35	36
2004	35	38	32	32	30	36	32	27	27	28	32	31

# Appendix D

## Solbergfoss River Inflow Data

Table D.1: Monthly mean inflow values at Solbergfoss ( $m^3/s$ ), provided by NVE.

	1	2	3	4	5	6	7	8	9	10	11	12
1902	138	117	111	196	813	1407	925	1039	1242	477	330	146
1903	96	111	179	369	1301	1994	1176	1147	1073	679	641	267
1904	167	145	114	343	1134	1875	848	522	416	248	230	119
1905	152	151	91	111	1055	1231	1216	861	693	473	326	195
1906	126	117	105	306	1639	1710	904	928	711	428	463	350
1907	191	136	163	369	1347	1968	1613	981	570	842	636	316
1908	193	150	130	314	1092	2021	1041	1059	855	520	277	175
1909	131	95	75	111	600	1818	1134	730	1086	882	687	342
1910	210	195	265	913	2120	1964	1173	995	634	472	344	251
1911	192	157	152	449	1949	1299	749	509	333	312	254	180
1912	156	132	176	312	1021	1404	817	1430	1407	527	308	342
1913	331	240	238	426	1950	1250	945	706	411	265	373	259
1914	226	260	220	516	1277	1044	1082	622	447	328	204	210
1915	191	195	213	404	864	1114	1237	1748	579	466	274	242
1916	227	202	179	481	2081	1804	1405	710	392	368	823	432

Table D.2: Continued monthly mean inflow values at Solbergfoss ( $m^3/s$ ).

	1	2	3	4	5	6	7	8	9	10	11	12
1917	245	249	213	201	613	1807	972	769	766	679	561	256
1918	225	211	204	396	997	890	1314	802	1101	1045	632	275
1919	248	226	207	406	1300	964	889	648	580	611	306	207
1920	201	230	344	1092	1660	1689	1239	1223	1058	464	226	229
1921	203	185	230	297	942	1123	665	713	629	436	308	217
1922	218	198	176	208	1037	1143	1100	1217	949	407	213	225
1923	242	223	214	237	836	1210	1254	936	927	972	752	270
1924	260	239	183	234	1123	1996	1762	1839	1322	952	531	327
1925	405	284	259	405	1160	1622	989	888	635	562	415	266
1926	268	259	254	510	1349	1942	1127	1117	715	685	858	446
1927	316	325	435	535	990	2331	2533	1681	1277	999	424	279
1928	259	249	226	315	1319	931	800	976	829	543	692	347
1929	248	240	232	309	961	1206	885	919	785	823	1010	733
1930	517	307	303	564	1468	1624	1356	1019	636	677	572	367
1931	290	270	252	301	1979	1577	1061	1058	408	369	579	295
1932	303	280	251	296	951	1333	994	786	433	701	332	470
1933	346	312	269	389	822	1273	804	739	449	505	352	226
1934	227	223	279	510	2246	1133	877	982	1453	1107	510	766
1935	367	344	348	544	1154	1570	1442	698	611	1135	1074	451
1936	422	402	371	552	1795	1404	1285	1297	611	287	380	376
1937	329	328	315	813	2068	1638	1160	695	563	360	351	286
1938	288	339	450	527	876	1257	1103	913	1188	1353	709	706
1939	389	416	414	566	1220	1742	2084	1415	551	301	276	281
1940	258	233	203	249	930	893	793	900	815	617	366	345
1941	330	306	290	266	479	759	784	918	735	373	303	265
1942	280	281	262	377	660	1119	918	766	727	738	666	411
1943	386	448	455	547	1372	1515	1123	782	663	558	499	377

Table D.3: Continued monthly mean inflow values at Solbergfoss ( $m^3/s$ ).

	1	2	3	4	5	6	7	8	9	10	11	12
1944	386	407	359	354	823	1969	1517	844	1070	1213	573	536
1945	430	439	463	715	1373	1639	1165	572	318	280	279	280
1946	278	292	312	606	907	1215	895	684	1321	657	436	526
1947	444	398	317	399	1167	971	920	377	303	266	257	249
1948	250	264	290	739	1142	944	991	637	1062	746	462	420
1949	431	423	389	519	1325	1822	943	665	500	586	597	448
1950	430	403	466	698	1422	1752	1352	1407	1239	884	469	386
1951	384	394	357	463	1463	1784	953	1507	1424	409	501	443
1952	471	412	385	502	1637	1219	1004	825	462	421	384	338
1953	325	327	347	575	1059	1473	1494	943	1081	651	666	451
1954	416	385	373	428	1141	1245	1021	1183	630	511	519	567
1955	431	432	376	340	688	1306	1164	504	345	350	362	345
1956	340	318	290	326	744	1188	910	714	999	607	410	354
1957	373	387	355	410	898	1313	1419	1324	1614	737	583	394
1958	359	335	304	311	667	1195	1144	784	507	880	578	384
1959	377	387	413	627	1833	856	610	420	347	293	398	484
1960	486	429	377	448	1212	1487	1659	995	625	707	532	511
1961	432	428	476	493	1192	1145	725	878	583	1202	1347	448
1962	427	431	366	459	1406	1308	1089	858	937	521	510	374
1963	370	329	298	415	1540	1139	927	1034	1001	823	561	407
1964	381	362	320	373	799	1007	1001	653	904	1362	546	414
1965	429	436	381	533	1111	1507	944	719	1296	596	424	363
1966	334	336	346	283	1976	1389	542	829	572	613	637	469
1967	481	462	563	561	1438	2447	961	677	618	1049	975	460
1968	474	437	429	728	1334	1373	950	432	428	360	423	403
1969	406	381	309	474	1290	1103	405	479	379	462	389	383

Table D.4: Continued monthly mean inflow values at Solbergfoss ( $m^3/s$ ).

	1	2	3	4	5	6	7	8	9	10	11	12
1970	367	336	290	326	1042	909	789	572	582	674	546	474
1971	482	490	384	493	1218	1243	972	677	394	375	378	374
1972	378	355	307	472	1063	1709	1235	696	430	354	328	343
1973	362	372	365	386	720	1314	1285	669	444	470	401	339
1974	351	402	420	576	932	734	742	484	863	799	577	486
1975	569	558	454	394	1406	884	615	401	385	698	509	458
1976	467	420	347	367	824	903	771	364	344	337	438	414
1977	402	371	355	398	1504	1395	669	451	428	399	653	435
1978	467	383	375	511	991	1037	683	467	471	461	429	366
1979	341	336	317	441	1049	1462	924	1190	658	614	489	405
1980	414	359	267	427	948	1212	993	607	653	891	492	448
1981	454	424	338	540	1313	1274	995	554	402	551	465	453
1982	408	392	383	606	1139	1179	689	490	352	568	542	507
1983	554	443	348	495	1770	1302	704	452	479	722	467	424
1984	447	385	296	480	1095	1389	702	622	473	1203	905	739
1985	550	419	368	400	1455	1449	1197	1290	1399	899	517	429
1986	436	345	288	322	1567	1071	451	733	556	403	543	595
1987	541	417	336	445	1379	1982	1187	674	846	1712	770	510
1988	545	535	395	496	1816	1534	938	928	1520	810	517	384
1989	421	444	567	680	1092	1137	842	1398	450	406	535	443
1990	463	718	586	667	1226	1106	1144	729	585	475	517	493
1991	478	340	382	724	553	750	911	574	376	483	514	485
1992	423	349	402	396	1106	1014	439	817	793	595	465	575
1993	539	460	347	365	1699	834	876	1363	669	688	547	517
1994	463	356	321	670	1381	919	869	670	716	475	432	511

Table D.5: Continued monthly mean inflow values at Solbergfoss ( $m^3/s$ ).

	1	2	3	4	5	6	7	8	9	10	11	12
1995	517	444	377	444	1080	2771	1036	560	393	318	396	400
1996	334	249	196	316	741	836	697	459	452	580	642	509
1997	461	371	370	318	1137	1295	1108	587	682	597	438	504
1998	525	434	411	530	1464	1123	1091	746	845	697	607	442
1999	483	389	385	901	1190	1689	1324	462	470	651	494	509
2000	532	467	368	556	1629	963	1455	709	579	1247	1881	1150
2001	668	515	377	524	1263	1032	1088	865	695	891	621	466
2002	442	528	421	752	1345	1316	1158	654	385	347	416	292
2003	315	304	290	484	1106	1045	760	682	516	481	401	485
2004	438	399	397	662	1118	603	682	496	755	814	492	536
2005	585	453	335	443	803	1121	955	820	593	473	958	618
2006	496	427	347	480	1487	847	459	618	620	735	995	1007
2007	688	587	525	604	1025	1083	1295	931	438	475	413	505
2008	639	547	556	657	1997	1380	798	828	530	529	593	633
2009	415	401	333	763	1153	787	1065	1243	981	520	581	630
2010	543	408	325	527	982	1089	925	952	907	997	543	421
2011	369	294	232	811	777	1682	1246	1542	1805	771	636	517
2012	509	507	499	630	1018	1177	1440	1314	772	721	914	583
2013	533	440	313	440	1474	1665	898	797	541	470	585	580
2014	699	654	816	721	1416	1421	785	722	552	900	1052	646
2015	521	542	570	579	1023	1190	1129	878	1217	582	498	571
2016	565	543	411	651	1056	1021	704	717	631	468	472	482
2017	503	417	369	497	926	1370	708	986	933	899	645	578



# Appendix E

## MATLAB Code

(Restricted Public Access.)